LIVERPOOL JOHN MOORES UNIVERSITY

LJMU Research Online

De Giudici, G, Medas, D, Cidu, R, Lattanzi, P, Rigonat, N, Frau, I, Podda, F, Marras, PA, Dore, E, Frau, F, Rimondi, V, Runkel, RL, Wanty, RB and Kimball, B

Assessment of origin and fate of contaminants along mining-affected Rio Montevecchio (SW Sardinia, Italy): A hydrologic-tracer and environmental mineralogy study

http://researchonline.ljmu.ac.uk/id/eprint/11338/

Article

Citation (please note it is advisable to refer to the publisher's version if you intend to cite from this work)

De Giudici, G, Medas, D, Cidu, R, Lattanzi, P, Rigonat, N, Frau, I, Podda, F, Marras, PA, Dore, E, Frau, F, Rimondi, V, Runkel, RL, Wanty, RB and Kimball, B (2019) Assessment of origin and fate of contaminants along mining-affected Rio Montevecchio (SW Sardinia, Italy): A hydrologic-tracer

LJMU has developed **LJMU Research Online** for users to access the research output of the University more effectively. Copyright © and Moral Rights for the papers on this site are retained by the individual authors and/or other copyright owners. Users may download and/or print one copy of any article(s) in LJMU Research Online to facilitate their private study or for non-commercial research. You may not engage in further distribution of the material or use it for any profit-making activities or any commercial gain.

The version presented here may differ from the published version or from the version of the record. Please see the repository URL above for details on accessing the published version and note that access may require a subscription.

For more information please contact researchonline@ljmu.ac.uk

http://researchonline.ljmu.ac.uk/

http://researchonline.ljmu.ac.uk/

LIVERPOOL JOHN MOORES UNIVERSITY

LJMU Research Online

De Giudici, G, Medas, D, Cidu, R, Lattanzi, P, Rigonat, N, Frau, I, Podda, F, Marras, PA, Dore, E, Frau, F, Rimondi, V, Runkel, RL, Wanty, RB and Kimball, B

Assessment of origin and fate of contaminants along mining-affected Rio Montevecchio (SW Sardinia, Italy): A hydrologic-tracer and environmental mineralogy study

http://researchonline.ljmu.ac.uk/id/eprint/11338/

Article

Citation (please note it is advisable to refer to the publisher's version if you intend to cite from this work)

De Giudici, G, Medas, D, Cidu, R, Lattanzi, P, Rigonat, N, Frau, I, Podda, F, Marras, PA, Dore, E, Frau, F, Rimondi, V, Runkel, RL, Wanty, RB and Kimball, B (2019) Assessment of origin and fate of contaminants along mining-affected Rio Montevecchio (SW Sardinia, Italy): A hydrologic-tracer

LJMU has developed **LJMU Research Online** for users to access the research output of the University more effectively. Copyright © and Moral Rights for the papers on this site are retained by the individual authors and/or other copyright owners. Users may download and/or print one copy of any article(s) in LJMU Research Online to facilitate their private study or for non-commercial research. You may not engage in further distribution of the material or use it for any profit-making activities or any commercial gain.

The version presented here may differ from the published version or from the version of the record. Please see the repository URL above for details on accessing the published version and note that access may require a subscription.

For more information please contact researchonline@ljmu.ac.uk

http://researchonline.ljmu.ac.uk/

*Revised manuscript with no changes marked

Assessment of origin and fate of contaminants along mining-affected Rio Montevecchio (SW Sardinia, Italy): a hydrologic-tracer and environmental mineralogy study.

Giovanni De Giudici[a,*], Daniela Medas[a], Rosa Cidu[a], Pierfranco Lattanzi[b], Nicola Rigonat[a], Ilaria Frau[c], Francesca Podda[a], Pier Andrea Marras[a], Elisabetta Dore[a], Franco Frau[a], Valentina Rimondi[d], Robert L. Runkel[e], Richard B. Wanty[f], Briant Kimball[g]

[a]Department of Chemical and Geological Sciences, University of Cagliari, Cittadella Universitaria, Monserrato, 09042 (CA - Italy)

[b]CNR-IGG, UOS Firenze, via La Pira 4, Firenze, I-50121, Italy

[c]Built Environment and Sustainable Technologies (BEST) Research Institute, Liverpool John Moores University, Liverpool L3 3AF, UK

[d]Dipartimento di Scienze della Terra, Università di Firenze, via La Pira 4, Firenze, I-50121, Italy

[e]U.S. Geological Survey, Colorado Water Science Center, 3215 Marine St, Bldg 6 Boulder, CO, 80303

[f]U.S. Geological Survey, MS 963 Denver Federal Center, Denver, CO 80225

[g]U.S. Geological Survey, 2329 W Orton Circle, Salt Lake City, Utah, 84117

Keywords: Hydrologic tracer techniques - Mine waters – Underground sources - Metal attenuation processes

*corresponding author

Abstract

Hydrologic tracer techniques were applied to Rio Montevecchio (SW Sardinia, Italy), a stream affected by mine drainage, allowing the calculation of discharge and contaminant loads. Discharge along the stream showed a constant increase throughout the 2.7 km-long study reach, up to 13.6 l/s at the last synoptic point. Calculated loads of mine-related constituents were large, reaching values of 1780 kg/day for SO_4^{2-}, 340 kg/day for Zn, 47 kg/day for Fe, and 50 kg/day for Mn. The difference of the cumulative instream metal loads between the first and the last synoptic sampling points indicated gains of 421 kg/day for Zn, 2080 kg/day for SO_4^{2-}, 56 kg/day for Mn, and 50 kg/day for Fe. The source areas critical for contaminants loading were almost all concentrated in the first 800 meters of the stream, with the exception of Pb, whose loading occurs evenly along the whole study reach. Precipitation of secondary minerals along the streambed was responsible for a very high attenuation of Al and Fe loads (66% and 77%) and affected also SO_4^{2-} and Zn loads, though less effectively.

Rio Montevecchio has the second highest metal load among the rivers investigated with tracer techniques in SW Sardinia. In comparison with Rio Irvi, which has one order of magnitude higher metal loads, natural attenuation processes limit the loads in Rio Montevecchio. Results are useful to clarify the hydrogeochemical paths involved in the release and attenuation of pollutants, improving our understanding of stream responses to contamination and aiding development of site-specific remediation actions.

1. Introduction

Besides a rich heritage of industrial archaeology (Orange, 2008), past mining activities have left behind vast and widespread amounts of wastes that result in deep and long-lasting modifications of soil and water quality at local to regional scales for an undetermined length of time. Contaminants are released into the environment by oxidative dissolution involving metal sulphide minerals still present in the orebodies and/or the materials present in the mining or metallurgical wastes (Cidu et al., 2018; Dold and Bernhard, 2014; Dunn, 1997; Lottermoser, 2010). These reactions can produce highly acidic waters, sometimes with extremely high concentrations of metals and sulphate, called Acid Mine Drainage (Caboi et al., 1999; Cidu and Fanfani, 2002; Nordstrom, 2011). Metals dispersed into the environment can interact with the biosphere (Ma et al., 2016; Merroun, 2007). This interaction is often responsible for natural attenuation of metal loads in streams affected by mining, through several processes (e.g. metal precipitation mediated by bacteria, metal stabilization at the soil-root interface and/or accumulation in vegetal tissues, etc.) (De Giudici et al., 2015, 2017b; Kothe et al., 2005; Larocque and Rasmussen, 1998; Medas et al., 2015, 2019), which are important for sustainable geo- bio-remediation technologies (De Giudici et al., 2017b). These studies point out the importance of the hyporheic zone, defined as the ecotone where geosphere, biosphere and water meet and where biogeochemical reactions take place (Byrne et al., 2014). The presence of dense riverbed vegetation was found to be a fundamental parameter for the development of biogeochemical barriers, because it promotes soil-root interactions, reducing trace-metal mobility and their dispersion (De Giudici et al., 2017b).

Hydrological tracer techniques have been developed to quantify the impact of mine drainage on a watershed scale (Buxton et al., 1997; Byrne et al., 2017; De Giudici et al., 2017a; Kimball et al., 2007, 2002; Rimondi et al., 2014). The spatial pattern of contaminant concentrations and pH in a stream results from the sum of all the contributions that can occur as visible surface inflows and subsurface inflow to the main stream flow (Kimball et al.,

2002). The combination of streamflow estimates with concentration data produces spatially-dense loading profiles (Runkel et al., 2013), that are used to identify sources of contaminants and stream segments where natural attenuation processes take place (Kimball et al., 2002). These estimates can be used to identify the provenance of metal loads and estimate priorities for remediation actions (Byrne et al., 2017).

In this study, a tracer-injection approach was combined with spatially detailed synoptic sampling to calculate river discharge, change of contaminants loads and to evaluate the impact of sampled inflows and unsampled underground sources on the stream chemistry (Kimball et al., 2002). The investigated area is located in the Montevecchio-Ingurtosu mining district (Arbus and Guspini municipalities, South Sardinia province, Italy). Mine drainages occur in two catchment areas geographically divided into East and West Montevecchio (Pisu et al., 2008). The West catchment was investigated by our group in a previous study (De Giudici et al., 2017a), and was found to have the highest loads of contaminants with respect to other streams draining mining-affected areas in the southwest part of Sardinia.

Environmental resiliency processes are defined as the ability of the environment to respond to stress or environmental pressure by, for the instance, any change in dominating cyanobacteria or sulphur reducing bacteria. Studying these processes in historical mine-affected rivers in southwest Sardinia can be effective to develop sustainable remediation strategies and technologies. Understanding microscopic processes of mineral dissolution and precipitation and assessing their effect at the watershed scale is best accomplished by coupling hydrological tracer techniques with geochemical and mineralogical studies. In the wider framework of the identification of the main pollution sources in the watersheds of the Iglesiente mining district and the study of the natural attenuation processes limiting the discharge of huge loads of contaminants in the Mediterranean Sea, this paper explores the impact of mine drainage from one of the biggest Zn-Pb mines in Sardinia to the Rio Montevecchio and the surrounding areas. Specifically, the aim of this paper is to complete investigation of main mine affected rivers in southwest Sardinia. Here we present the results of a hydrologic-tracer experiment in Rio Montevecchio (East catchment), which receives discharge from inflows draining the Piccalinna impoundment and the tailings downstream, to assess the sources of contaminants and identify potential attenuation processes along the stream. In Rio Montevecchio, mine tailings and river sediments have been transported to and deposited onto the riverbed for more than 30 years, in contrast to Rio Irvi where erosional processes dominate (De Giudici et al. 2018). This work provides a comparison between the two catchments belonging to the Montevecchio mining district - Rio Montevecchio and Rio

Irvi (De Giudici et al., 2017a) - to highlight the differences in loading sources, attenuation processes, hydrology and seasonality that will affect the remediation strategies to be applied in the two watersheds. This study confirms that active sedimentation on the riverbed can cause a decrease in metal load by one order of magnitude. The investigation technique and results from this study are widely applicable to other case studies all over the world and should help inform actions regarding riverbed remediation.

2. Field area

In the Sulcis-Iglesiente-Arburese district (southwestern Sardinia, Italy), mining has been the main economic activity for centuries, until the final shutdown of the hard-rock mines between 1980 and 1992. Around 70 million m^3 of flotation muds and other mining wastes were left abandoned there (Romano et al., 2017), resulting in contamination of surface waters (Cidu and Fanfani, 2002; Pisu et al., 2008).

Rio Montevecchio has its origin near the village of Montevecchio, located within the old mining district of the same name. The first mining works in Montevecchio date back to Phoenician and Roman times; a boom in extraction activity started in 1842, and ceased officially in 1991. The mine mainly produced Pb and Zn, with a cumulate production close to 3 Mt metal; Ag also was an important product (ca. 1000 t), along with several other byproduct metals (Bi, Cd, Co, Cu, Sb, and Ge). The main ore minerals were galena (PbS) and sphalerite (ZnS), often accompanied by pyrite (FeS_2) and chalcopyrite ($CuFeS_2$) in a gangue of siderite ($FeCO_3$) and quartz (SiO_2), with minor barite ($BaSO_4$) and calcite ($CaCO_3$). The mineralized bodies consist of a set of veins extending for at least 10 km westward to the Ingurtosu mining district. The veins are hosted mainly in silicate rocks of the Paleozoic basement (Ordovician-Silurian schists and metamorphosed sandstones of the autochthonous unit; Cambro-Ordovician low-grade metamorphosed volcanites and sediments of the allochthonous “Arburese” unit), and subordinately in the Variscan Arbus granodioritic pluton (303.7±1.1 Ma, (Cuccuru et al., 2016)).

A network of shafts built during underground mining to exploit the 10 km long vein system was flooded by groundwater after the closure of the mines. As a result, waters now flow from adits, notably Casargiu (the inflow of Rio Irvi on the West side), and the two drainage galleries at Montevecchio that are the source of Rio Montevecchio. Other adits that are not visible are buried at the bottom of the Piccalinna impoundment and are the source of the

water that flows through the impoundment itself to the Rio Montevecchio (IGEA, internal report).

The superficial hydrology of the study area is dominated by Rio Montevecchio, whose spring is the drainage gallery "Gallery n°173" (referred in this study as MV-0, and as MV5 by Cidu et al., 2011) and Rio Struvoniga (Fig. 1). After Rio Struvoniga, the main inflow is R3 (RBI-283), originating at the drainage gallery Piccalinna n°172, and referred to as MV4 (Fig. 1) by Cidu et al. (2011). Rio Struvoniga converges in Rio Montevecchio near the SSE corner of the Piccalinna impoundment, approximately 800 meters from the mine adits discharging their waters in Rio Montevecchio. Both streams have perennial fluvial regimes, being supplied by natural springs; however, they are also affected by the discharge from mine adits and spillages from the Piccalinna impoundment (Fig. 2). Discharge at the bottom of the Piccalinna impoundment was estimated to vary with seasons between 2 and 20 l/s (Caboi et al., 1999; Cidu, 2011).

Climate in Sardinia is characterised by long periods of heat and drought, usually extending from May to September, interrupted by a short rainy season, with occasional heavy rain events that have occurred more frequently in the last decade. The mean rainfall in the Montevecchio area is estimated at 727 mm/year, with a mean of 50 rainy days per year (Bacchetta et al., 2007). The mean annual temperature is 16°C (Cao Pinna et al., 1998).

3. Materials and Methods

3.1 Core Extraction and XRPD analysis

To define the processes that contribute to instream loading and/or attenuation, three cores, between 30 and 100 cm long, of tailing deposits were extracted from the riverbed using a core sampler (Atlas Copco's COBRA), that allowed the recovery of undisturbed samples in sealed plastic bags; furthermore, several specimens of efflorescent salts (Fig. S1 and S2) were collected along the river. After drying at room temperature, the material was lightly ground in an agate mortar and subjected to X-ray powder diffraction (XRPD) analysis, using conventional θ-θ equipment (PANalytical X'Pert Pro) with Ni-filtered Cu $K\alpha_1$ wavelength radiation (1.54060 Å), operating at 40 kV and 40 mA, using the X'Celerator detector. The resulting patterns were processed using the X'Pert HighScore Plus software (PANalytical B.V., Almelo, The Netherlands) to identify the mineral phases present.

3.2 Tracer Techniques

In this study, a mass-loading approach (Kimball et al., 2002) already successfully applied in nearby watersheds (De Giudici et al., 2017b, 2017a, 2014), is used to quantify metal loads. This method allows quantification of influx of metals from various sources and the extent of geochemical processes in the stream to provide a science-based support tool for decisions on environmental remediation of stream catchments that include abandoned mines (Runkel et al., 2013). More details on the technique and its development are available in De Giudici et al., 2018; Kimball et al., 2002; Runkel et al., 2013 and references therein.

Between May 30th and June 3rd 2013, the University of Cagliari and the United States Geological Survey (USGS) ran a field campaign along Rio Montevecchio using hydrologic-tracer techniques. For this study, NaBr was used as the tracer salt. The rate of injection and the Br concentration of the injectate were determined by collecting the volume for a given number of 10-second pulses. The mass of that injected volume was measured, and its specific gravity provided the concentration and the volume (De Giudici et al., 2017b). In Rio Montevecchio a NaBr solution of 199 g/l Br (RSD 0.7%) was injected at a rate of 31 ml/min (RSD 0.11%) for 94.5 hours before the synoptic sampling. Tracer-dilution methods are thoroughly described by Kimball et al. (2002).

On June 3rd 2013, a tracer slug was injected along Rio Sitzerri near the SP 4 road bridge. A slug injection allows for an instantaneous discharge measurement that does not imply the saturation of the hyporheic volume and is used to detect water gain or loss along the study reach (Lambert et al., 2011). Two other slug injections were performed on May 25th 2015 at points MV-1182 and T5 (MV-3850). In particular, during the Rio Sitzerri slug injection, water was collected and flow initially estimated using a graduated bucket, considering the low flow along that part of the stream.

3.3 Water sample collection and analysis

Along the 2.7 km-long study reach of Rio Montevecchio, 29 stream sites and 8 inflows (either left – LBI- or right -RBI- bank inflows) were selected for synoptic sampling (Fig. 1). Five sites were selected as transport sites (T sites), where water samples were collected frequently to monitor transport of the tracer in each part of the stream, and to monitor the plateau concentration of the tracer.

Synoptic sampling of the stream points was carried out on June 3rd 2013, starting at 11 AM, after the tracer concentration reached a plateau at all 5 of the T sites. Sample processing was carried out in a field laboratory the same day of sample collection. At each sampling point, 1L of sample was collected from which four aliquots were sub-sampled: a 0.45-μm filtered,

unacidified sample for major ions analysis by ion chromatography (IC, Dionex ICS3000), two 0.45-µm filtered aliquots acidified to 1% v/v with high purity HNO_3 for metal determination by inductively coupled plasma optical emission spectroscopy (ICP-OES, ARL Fisons 3520) and inductively coupled plasma mass spectroscopy (ICP-MS, PE-ElanDRC), and an unfiltered aliquot acidified to 1% v/v with high purity HNO_3 for total-recoverable metals analysis (Taggart, 2002). Moreover, in the field laboratory an unfiltered and unacidified aliquot was used to determine the pH of solution (using Orion® pH meter and Orion Ross® electrode), the redox potential (Eh, using a platinum electrode, and correcting values against the Zoßell's solution; Nordstrom, 1977), and to measure alkalinity by Gran titration. The detection limit (DL) for chemical analysis was calculated at 10 times the standard deviation of the blank solutions. The accuracy and precision of trace-element determination were evaluated with two reference solutions: the NIST SRM 1643e and the EnviroMAT Drinking Water, High EP-H-3 and Low EP-L-3. Rhodium was used as an internal standard for ICP-MS analysis to correct for instrumental drift. As confirmed using PHREEQC software (Parkhurst and Appelo, 1999), the ionic charge balance was always better than ± 10%.

Saturation indices (S.I.) and calculated speciation by PHREEQC (Parkhurst and Appelo, 1999) reported here refer to chemical species determined in the aqueous fraction <0.45 µm. Following a previous study by Cidu et al. (2011), geochemical modelling by PHREEQC was carried out using the 'wateq4f.dat' database implemented with the solubility constants (at 25°C) of geological and biological hydrozincite (Eq. 1), after Medas et al. (2014), hemimorphite (Eq.2) (Cidu et al., 2011) and three relevant Fe and SO_4 bearing phases: SO_4-bearing green rust (Eq. 3) (Frau et al., 2015), schwertmannite (Eq. 4), and two-line ferrihydrite (Eq. 5) (Majzlan et al., 2004).

Eq. 1: $Zn_5(CO_3)_2(OH)_6 + 6H^+ \rightleftharpoons 5Zn^{2+} + 2CO_3^{2-} + 6H_2O$ log k = 6.2 (geo)
log k = 9 (bio)

Eq. 2: $Zn_4Si_2O_7(OH)_2 \cdot H_2O + 8H^+ \rightleftharpoons 4Zn^{2+} + 2H_4SiO_4 + 2H_2O$ log k = 21.8

Eq. 3: $Fe_4^{II}Fe_2^{III}(OH)_{12}SO_4 \cdot 8H_2O \rightleftharpoons 4Fe^{2+} + 2Fe^{3+} + 12OH^- + SO_4^{2-} + 8H_2O$
log k = -134.4

Eq. 4: $FeO(OH)_{0.75}(SO_4)_{0.125} + 2.75H^+ \rightleftharpoons Fe^{3+} + 0.125SO_4^{2-} + 1.75H_2O$ log k = 1.2

Eq. 5: $Fe(OH)_3 + 3H^+ \rightleftharpoons Fe^{3+} + 3H_2O$ log k = 3.7

3.4 Mass-balance calculations

Metal loads (M) were calculated by multiplying streamflow estimates (Q_x) by constituent concentrations (C_x) at each synoptic point x by the following equation $M=C_x*Q_x$, to obtain estimates of constituent "sampled" load (converted to kg/day), the primary quantity used to identify metal sources along the entire study reach (Runkel et al., 2013).

A stream segment is defined as the distance between two sampling sites; the changes in metal load in one segment provide the basic information to identify sources of metal load (positive ΔM_s) or places where attenuation processes take place (negative ΔM_s). The change in sampled load occurring in a stream segment is defined as $\Delta M_s = C_D Q_D - C_U Q_U$ (Kimball et al., 2002), where C represents the contaminant concentration and Q the discharge at any pair of synoptic points respectively downstream ($_D$) and upstream ($_U$).

The instream load is calculated by summing the load values at any point, giving the *"instream"* load profile. The cumulative instream load is calculated by summing the positive values of ΔM_S at any point, giving the *"cumulative"* load profile.

The change in load that can be attributed to surface water and groundwater from each inflow (Table S1) is calculated as $\Delta M_i = C_i(Q_D - Q_U)$, where Ci is the sampled concentration of water from the inflow and values of Q come from stream sites downstream ($_D$) and upstream ($_U$) from the inflow. Where no inflows are present, ΔM_I assumes zero value; this is called *"inflow*" load and the sum of its values gives the *"inflow"* load profile.

The difference between the cumulative load and the inflow load is an estimate of the amount of dispersed groundwater loading along the study reach. The difference between the cumulative load and the instream load, at the end of the study reach, indicates the net attenuation of the constituent along the entire study reach (De Giudici et al., 2017a).

3.5 Statistical analysis

To define groups of chemically-related instream samples and hence divide the stream into meaningful sub-reaches, cluster analysis was performed. Principal components analysis (PCA) was carried out to understand the relationships between the chemical components to help describe sources and fate of contaminants. The PCA analysis was performed with free software CoDaPack (Comas-Cufì and Thiò-Henestrosa, 2011) and was coupled with cluster analysis (Ashley and Lloyd, 1978; Templ et al., 2008) performed with Origin 2015 (OriginLab Corp., Northampton, MA 01060, USA). Hierarchical cluster analysis (CA) was performed using the furthest cluster method in Euclidean space, after identifying the possible number of groups based on the geologic, hydrologic or geochemical information gathered in the field or in the laboratory. To avoid spurious correlation when multivariate statistical

methods are applied to compositional data (Aitchison and Greenacre, 2002; Biddau et al., 2019), the centered log-ratio (clr) transformation was performed, following the formula in Eq. 6.

Eq. 6: $clr\ (x)i = ln\frac{(x)i}{g(x)}$

Where (x)i is each component, and g(x) the geometric mean of all considered components.

When the dataset included non-detected or previously-defined below-detection limit concentrations, the DL values were used. The results of the centered log-ratio transformations are shown in the compositional clr-biplot (Biddau et al., 2019; Pawlowsky-Glahn and Buccianti, 2011), where samples are divided into clusters identified by the CA; statistical analysis was performed either on compositional or loading data. Clr-biplot allows easier analysis of geochemical variables because the length of the vectors and the angles between the vectors and between links can be statistically interpreted (Pawlowsky-Glahn and Buccianti, 2011).

4. Results

4.1 Mineralogy of the flotation muds and tailing deposits

Approximately three quarters of the volume of the mining wastes of the Piccalinna impoundment is flotation muds (with a high percentage of sandy mining products; PROGEMISA, 1998). These materials are characterised by high metal concentrations, exceeding values of 9,000 mg/kg for Zn, and 4,000 mg/kg for Pb (Pusceddu, 2013). XRPD analysis of the samples collected from the cores extracted from the Piccalinna impoundment shows that the dominant phases are quartz, muscovite and siderite, and primary sulphides, sphalerite, galena and pyrite, substantially reflecting the mineral assemblage of the ore veins and host rocks (Pusceddu, 2013). Oxidation and weathering products such as sulphates, oxides and carbonates are widespread in samples collected from surface outcrops and from short core wells. Efflorescent salts were found both in surface outcrops, tailings and core wells. During dry seasons, evaporation-driven precipitation of white crusts on the Rio Montevecchio riverbed has been observed. Gypsum and jarosite were the dominant recognized phases, the former mainly found on exposed surfaces and the latter in the tailings, riverbed precipitates and subsurface pockets immediately below gypsum layers. These phases indicate high reactivity of primary minerals in the tailings and along the riverbed.

4.2 Water chemistry

Tables S2-S3 report distance (m), pH, major and trace chemical components in filtered water samples of the Rio Montevecchio. The corresponding data for the inflows are reported in the supplementary material (Table S4 and S5). All components refer to 0.45 μm filtered samples (dissolved components). Unfiltered, or total recoverable, Fe concentrations also are included. The pH (Fig. 3a) instream spatial profile shows a constant decrease from 5.9 to a minimum value of 4.02 in the first 800 metres of the study reach due to acidic inflows like R1, R2 and R3. A constant increase (pH 4.7-5) characterised Sub-reach 4, due to the buffering effect of carbonate minerals hosted in the Eocene limestones interacting with the inflows R4, L2, R5 and R6.

Figure 3b shows a modified Piper diagram used to classify waters from Rio Montevecchio and its inflows. Zinc is included as one of the major cations because of its high concentrations. Sulphate is the dominant anion in all the samples collected along the stream, whereas cationic composition changes from a prevalent Zn-Ca composition to a dominant Ca-Mg composition proceeding downstream (red arrow in Fig. 3b). The waters from the inflows have a heterogeneous composition and they can be divided into two main groups: the largest one (group 1 in Fig. 3b - triangles inside the red ellipse) with a Zn-Ca-(Mg)-SO_4 composition, and the second (group 2 in Fig. 3b - triangles inside the blue ellipse) with a composition ranging from Mg-Ca-SO_4 to Na-Ca-Mg-HCO_3-Cl. Inflows characterised by a dominant Zn-Ca-(Mg)-SO_4 composition all occur within the first 612 m of the stream (see Table S4), suggesting that surface waters of these inflows contribute to the previously described variations in water chemical composition along the Rio Montevecchio.

4.3 Contaminant concentrations

The main contaminants (Fig. 4a-f) in waters from Rio Montevecchio are Zn (250-630 mg/l), Mn (9-63 mg/l), Fe (0.4-83 mg/l in the dissolved fraction, 1.9-90 mg/l in the total fraction), Cd (2,000-4,600 μg/l) (Table S3), and Pb (850-2,000 μg/l). These constituents had concentrations well above the freshwater pollution thresholds (as defined by Italian regulations, D.lgs 152/2006: Zn 0.5 mg/l, Mn and Fe 2 mg/l, Cd 20 μg/l, and Pb 200 μg/l). Instream SO_4^{2-} concentrations, with the exception of MV-0, are always above 1,000 mg/l, whereas SO_4^{2-}concentrations of the inflows are extremely variable, from 32 mg/l to 4,800 mg/l (Table S4). Aluminium had the highest concentrations in the first 700 meters (1,300-2,900 μg/l), exceeding the freshwater pollution thresholds according to D.lgs 152/06 (Al 1,000 μg/l) then decreased until the end of the investigated stream section, ranging from 210 to 540 μg/l. Iron, Pb and Al showed a great difference between concentrations in the non-

filtered (total-recoverable metals) and filtered samples (Fig. 4c,e,f), reflecting the presence of Fe-, Al- and Pb-bearing colloids in the Rio Montevecchio waters, thereby testifying to the high affinity of these three metals with colloids present under these conditions. Zinc (Fig. 4b) is reactive too, although the differences between the two curves suggest that it might have a lower affinity with the colloidal fraction. Mn (Fig. 4d) had nearly identical spatial profiles of dissolved and total concentrations, hence it does not form colloids in these waters (Runkel et al., 2013).

4.4 Statistical analysis

The clr-biplot (Fig. 5) shows the Rio Montevecchio instream waters (a) and inflow waters (b) components in multivariate space. The apparent components were the major ions and trace metals shown in Tables S2 and S3 and Tables S4 and S5 and the clustering of individual sample observation based on the results of hierarchical CA analysis shown in Fig. S3. Regarding the instream waters, the first component accounted for 61% of the Euclidean variability and the second component for 29% (Fig. 5a). The longest vectors from the origin (Fig. 5a) were Fe and Al, followed by Mn, Cd and Cu, indicating that the ratio of concentration of these contaminants is the most variable across the samples. The shortest vectors from the origin were Co, Ni and SO_4, meaning that the ratio of concentration of these contaminants to the others is the least variable. The longest links between vectors were between Fe and HCO_3 and Al and K, to indicate that these two couples of elements had the strongest reciprocal ratios.

The strongest correlation observed in Fig. 5a was among Cu, Cd and Zn (fourth quadrant) and Ca, Mg and SO_4^{2-} (second quadrant), indicating that the ratio of these elements was nearly-constant and their corresponding abundances are strongly correlated (Aitchison and Greenacre, 2002). The SO_4^{2-} vector was orthogonal to Fe and HCO_3, suggesting that the relative abundance of these contaminants is not correlated (Aitchison and Greenacre, 2002).

The Rio Montevecchio samples could be divided into five groups (Fig. S3 and Fig. 5a. The first, called Injection point, contained the MV-0 sample which is affected by the drainage gallery “Gallery n°173”. The second cluster (Sub-reach 1) comprised the first two synoptic points, unaffected by visible inflows but where the highest Cu, Cd and Zn variation was recorded. The third cluster (Sub-reach 2) comprises the synoptic samples collected in the stream reach severely affected by the inflows with the highest concentrations of pollutants (Table S4 and S5), where the highest Al variation was observed. The fourth cluster (Sub-reach 3) contained the samples collected in the stream section with no visible inflows and

closer to the Piccalinna impoundment slope, where the highest variation of Fe was visible, and the final cluster (Sub-reach 4) includes all the samples collected downstream from the confluence of Rio Struvoniga with Rio Montevecchio.

Water samples from the inflows featured a different behaviour, with no clear clustering of the samples (Fig. 5b). Component 1 contributed 63% and component 2, 19% of the Euclidean variability. The strongest correlation (Fig. 5b) was between Ca, Cd, Mg and Fe (second quadrant) and SO_4^{2-} and Mn (third quadrant). HCO_3, Na and Cl showed a good correlation too, consistent with the results shown in Fig. 3. The highest variance can be seen for Pb, Al, Zn and Mn, and the lowest for Ca, Mg and K.

4.5 Streamflow by Tracer-Dilution

The Br background concentration measured upstream from the injection point was less than 0.6 mg/l, while at the first site downstream from the injection the Br concentration reached 75 mg/l, and then decreased downstream, due to dilution from inflows. At the end of the study reach, the concentration was 7.6 mg/l. Figure 6 shows the downstream profile of Br concentration and the calculated discharge profile. Discharge increased by less than 1 l/s in the first 150 metres of the reach; then quickly surged over the next 600 metres, in which all the inflows and underground sources related to the Piccalinna impoundment are located, to reach 10.1 l/s at the synoptic point immediately downstream of Rio Struvoniga (L2). In the last part of the reach, the discharge increased by less than 4 l/s.

4.6 Loading Analysis

Based on the calculated discharge and the measured concentrations of metals and SO_4^{2-} provided in Tables S2-S5, load profiles of filtered SO_4^{2-}, Mn and total-recoverable Zn, Al, Pb and Fe were calculated, together with filtered Fe (Fig. 7a-f).

The SO_4^{2-} instream load reached a value of 1780 kg/day, and the cumulative load 2040 kg/day (Fig. 7a); 58% of its cumulative load was gained before L2 in the first three sub-reaches with Sub-reach 2 accounting for 38% of the cumulative load. The segment 300-387 meters is the largest source area for SO_4^{2-} (13% of cumulative load), followed by the 262-279 segment (8.7%), which was affected by inflow R3, and segment 799-819. The SO_4^{2-} load increased constantly along the entire stretch of the study and attenuation processes accounted for 15% of the load (Table S6).

The Zn instream load was fairly high, attaining a maximum value of 340 kg/day (Fig. 7b). The cumulative Zn load of Rio Montevecchio was 421 kg/day (Fig. 7b), and 53% of this load was gained before L2, with Sub-reach 1 accounting for the biggest statistical variance (Fig. 5a). The segment 262-279 was the largest source area for Zn (17% of cumulative load), followed by 300-387 (12.6 %) and 1745-1886 (11.3 %) segments. Zn load attenuation was calculated at 19% of the cumulative load, suggesting a low affinity for solid phases of this ion. Among the considered contaminant loads, Zn was the least variable through the dataset (Fig. 5a-f).

Like Zn, Mn had a very low affinity for solid phases, resulting in only 20% attenuation on a cumulative load of 56 kg/day (Fig. 7c). Most of the Mn variability was related to reaches 3 and 4 (Fig. 7c), with the main source area being segment 300-387 (23% of the cumulative load).

The loading patterns of Fe (Fig. 7d) indicated that the biggest loading increase occurs in Sub-reach 3, with segment 300-387 being its main source area (43% of the cumulative load). Loads begin dropping 600 metres downstream from MV-0, constantly decreasing throughout all of Sub-reach 4, marked in the field by a red-orange Fe precipitate along the streambed, testifying that Fe is extremely reactive especially in the last sub-reach. The cumulative load of total recoverable Fe is 50 kg/day, and 47 kg/day for filtered Fe; the apparent total amount of colloidal (>0.45μm) Fe is therefore 3 kg/day. The total attenuation along the stream is 70 and 77% for total recoverable and filtered Fe respectively (Table S6).

The pattern for Al (Fig. 7f) shows that its main source area corresponds to the segment 262-279 (15%), besides the shaft MV-0 (which accounts for 48% of the cumulative load), A progressive attenuation of its load occurred, like Fe, especially in Sub-reach 4. The total attenuation of Al is 66% (Table S6) on a cumulative load of 1.3 kg/day.

PCA analysis (Fig. 5) showed that vectors of Fe and Al are the longest, confirming their highest variability throughout the loading dataset, but were also almost orthogonal, suggesting that their relative abundances were not well correlated.

Lead showed overall low loading values (less than 2.5 kg/day), with an increasing trend throughout the entire study reach, but more pronounced beyond 600 metres, suggesting the presence of additional sources of this contaminant in Sub-reach 4 (Fig. 7e).

The results of discharges calculated with the slug injection along Rio Sitzerri on June 3rd, 2013, gave a value of 4.8 l/s, with load values of 84.8 kg/day Zn, 4.3 kg/day Mn, 0.2 kg/day Fe and 0.12 kg/day Pb. Such a great discrepancy in river discharge compared to the value

calculated at MV-2800 (13.55 l/s), which is located 2 km upstream, was backed by visual evidence throughout the late spring and summer. It is not uncommon to observe that there is flow along Rio Montevecchio even though Rio Sitzerri may be stagnant or dry. This observation is consistent with the fact that downstream from our lowest synoptic point, sub-riverbed flow is common.

The results of the slug injection in 2015 showed a discharge value of 6.1 l/s at MV-1182 and 8.8 l/s at MV-3850. In particular, the comparison of discharge data between the MV-1182 slug of 2015 and the data from the synoptic point MV-1133 (Table 1) showed that in two years-time, in the same season, the discharge was reduced by 45%, but the concentrations of contaminants were almost the same (±7%). This result suggests that the seasonal and/or yearly difference in loads depend mainly on the hydrological regime and on the abundance of rainfall.

The hydrology of the Rio Montevecchio-Rio Sitzerri watershed affects pollutant transport to the lagoon of Santa Maria, which is 40 Km downstream from the Piccalinna impoundment. Comparing the discharge at the last synoptic point and at the slug injection point downstream along Rio Sitzerri, a loss of water greater than 60% was observed. The flowpath for this lost water was not further investigated in this study.

5. Discussion

5.1 Discharge loads and mineral-water interaction processes.

Instream samples show a substantial variation in the main cation composition (Fig. 3) that may be due to water-rock interaction and/or to surface or groundwater inflows. In fact, inflow waters show a different main cation composition, with a clear division of the samples in two groups: one with a water chemistry similar to the instream samples, the other a different one that can be explained by the interaction of groundwaters with the Eocene limestones, containing NaCl-rich pockets, present at the bottom of the Piccalinna impoundment.

Rio Montevecchio had calculated instream loads of SO_4^{2-} greater than 1700 kg/day, Zn around 300 kg/day, and Mn around 45 kg/day. The cumulative contribution of unsampled underground sources is very large (over 70 % for all contaminants). The vast majority of Rio Montevecchio loads were acquired in the first 800 meters, directly influenced by the waters coming from the aquifer (PROGEMISA, 1998) hosted in the Piccalinna impoundment (51% Pb, 52% Zn, 58% SO_4^{2-}, 55% Cd, 67% Mn, 74% Fe and 83% Al). This is due to the release

of contaminants from the metal sulphides still present in the Piccalinna waste and fed to the river by visible tributaries and unsampled discharging groundwaters, whereas for Rio Irvi more than 65% of the loads of all contaminants come from the Casargiu adit alone. The main source areas of contaminants were identified as the segment 300-387 (main source for SO_4^{2-}, Mn, Fe, and second most important source for Zn), followed by the segment 262-279 (main source for Zn, Cd and Cu and second source for SO_4^{2-} and Al), which is characterised by the presence of inflow R3 (MV-4 in Cidu et al., (2011)). The shaft Piccalinna n°172 (here MV-0 and MV-5 in Cidu et al. (2011)) was the main source area for Al. Pb loading occurred evenly along the entire stream course.

The calculation of the S.I. (Table S7) of the principal Fe-bearing phases using PHREEQC showed that the waters in Rio Montevecchio are undersaturated in green rust II (GRII, S.I. < -5) but oversaturated in ferrihydrite, schwertmannite and jarosite ($0 \leq$S.I.≤ 6). However, apparent oversaturation in ferrihydrite and schwertmannite is likely an artefact caused by colloids passing through the filter (Nordstrom, 2011). Attenuation of Fe along the stream could be mainly attributed to the formation of Fe oxyhydroxides. Saturation indexes for Fe oxyhydroxides (Table S7) indicate saturation in phases which are generally metastable. This result is consistent with the initial precipitation of schwertmannite and ferrihydrite, which are later transformed into stable microcrystalline goethite (Bigham and Nordstrom, 2000; Schwertmann and Taylor, 1972). Reasonably, attenuation of Zn was driven by absorption on Fe-bearing precipitates or jarosite (Forray et al., 2014; Kerolli-Mustafa et al., 2015). Despite the waters being saturated in anglesite (Table S7), this phase was not detected in the samples analysed by XRPD, so Pb attenuation can be related to the precipitation of plumbojarosite (Frantisek, 2008) or absorption on jarosite (Figueiredo and da Silva, 2011). Saturation indexes indicate oversaturation for alunite and undersaturation in amorphous $Al(OH)_3$ along the entire study reach and saturation in gibbsite (Table S7) in Sub-reach 4, where most of the Al attenuation occurred.

Minor jarosite and Fe-sulphates were observed in the riverbed, stream sediments and tailings, often associated with gypsum in dry sediments (Fig. S2b-c) and seldom with goethite (S2b), in amounts subordinate to the predominant riverbed red-coloured Fe-oxyhydroxide precipitates. Jarosite is a ferric hydroxysulphate, one of the last-forming secondary minerals after the oxidative dissolution of pyrite and, likely, other Fe-rich metal sulphides (Jerz and Rimstidt, 2003, and references therein). It can absorb and later release metals (Desborough et al., 2009; Kerolli-Mustafa et al., 2015) due to its instability especially at higher pH values,

where it is transformed into more stable Fe oxyhydroxides or oxides (Arslan and Arslan, 2003; Bladh, 1982; Elwood Madden et al., 2012). Jarosite has relatively low solubility (Baron and Palmer, 1996) and is more stable at higher pH values than the efflorescent salts (Jerz and Rimstidt, 2003). Its formation is related to processes occurring during drought seasons, which cause lowering of the water table with sediment exposure and evaporation of shallow groundwater (Cavanagh et al., 2017). In this study, jarosite was found in immediate subsurface sulphate pockets related to gypsum on the Piccalinna banks, but also in wet or water-saturated stream sediments and tailings. Therefore, we related its formation to evaporation processes occurring during drought season, involving either Rio Montevecchio stream waters or shallow groundwater. In the rainy season, the water table rises again, causing the quick dissolution of the most soluble efflorescent salts (e.g. gypsum), but preserving jarosite, that is less prone to dissolution, in water-saturated sediments and tailings.

5.2 Principal component and multivariate analysis.

PCA analysis facilitated a better understanding of the relationships among the contaminants. The compositional clr-biplot (Fig. 5a) clearly showed how instream Cu, Zn and Cd are highly correlated with each other, suggesting that the origin of their loads is related to oxidative dissolution of primary sulphides still present in the Piccalinna waste (Dold and Bernhard, 2014; Dunn, 1997); in fact, the highest concentrations of these metals were measured in the first 300 meters of the river, where Rio Montevecchio receives contributions directly from the aquifer of the Piccalinna impoundment. Pb was less correlated to these metals, because the highest concentrations were observed in other sectors of the stream, likely sourced from discharging groundwaters interacting with the tailings downstream. Notably, Fig. 5a shows how the low instream Euclidean variability of SO_4^{2-} was related to Ca, Mg and K, suggesting that the main source of this contaminant might be related to the dissolution of efflorescent salts (Jerz and Rimstidt, 2003) rather than dissolution of primary sulphides. The observed high SO_4^{2-} concentrations result from its high mobility and conservative character. Iron and Al showed high Euclidean variability, but they were not correlated, suggesting that the loads originate from different sources and the attenuation processes were ruled by the precipitation of different mineral phases.

Sampled inflows (Fig. 5b) showed a completely different behaviour than instream samples, with SO_4^{2-} more correlated to Zn and Mn. In contrast Ca and Mg were more closely correlated to Cd and Fe, with HCO_3 lying between the previous group and Cl and Na. This

result might indicate that inflows mainly derive their loads of SO_4^{2-} and Zn from dissolution of primary sulphides and Ca, Mg, Cd and Fe derive from possible dissolution of carbonate-bearing minerals.

5.3 Comparison with neighbouring Rio Irvi catchment

Rio Montevecchio and the previously investigated Rio Irvi (De Giudici et al., 2017a) are fed by flooded mine adits located in two different watersheds, respectively Montevecchio Levante (east) and Ponente (west), but belonging to the same vein system. Despite this common feature, these streams showed substantial differences in loads and mineral-water interaction processes. In Rio Irvi Zn and SO_4^{2-} attain peak loads of 2000 and 7460 kg/day respectively, whereas in Rio Montevecchio Zn and SO_4^{2-} had much lower load maxima (Zn: 300 and SO_4^{2-} 1700 kg/day).

The discharges of the two streams were similar, attaining around 25 l/s at their maxima; however, Rio Irvi, after the adit at the Casargiu shaft, had little variability in discharge and contaminants loads, whereas Rio Montevecchio gradually reached the maximum discharge and loading values due to visible tributaries and unsampled underground waters coming from the Piccalinna impoundment and mine tailings downstream. The Rio Montevecchio riverbed is characterised by a persistent thick layer of mine waste and sediments, while sediments in Rio Irvi riverbed are not abundant (De Giudici et al., 2017a), due to its prevailing erosional regime. This, coupled with a different hydrological regime of the two streams, with Rio Montevecchio more affected by seasonality and drought events, affects the natural attenuation mechanisms and the observed mineralogical reactions. Furthermore, the presence of a thick riverbed sediment cover along Rio Montevecchio is potentially highly beneficial for the growth of vegetation and hence the creation of resilient and effective biogeochemical barriers.

6. Conclusions

In this study we reported an investigation on Rio Montevecchio applying hydrological tracer techniques. Contaminant loads in Rio Montevecchio derived from seepage from the Piccalinna impoundment (stream reach from 0 to 700 m) and from tailings in riverbed and banks (from 700 m to the end of the reach). Natural attenuation of dissolved Fe and Al was observed. PCA analysis confirmed that large proportions of the loads of Zn, Cd, Cu and Pb are fed to the river by waters interacting with primary sulphides still present in the Piccalinna

waste. Statistical analysis also confirms that SO_4^{2-} is correlated to Ca, Mg, and K. We attributed this correlation to the formation and/or dissolution of efflorescent salts. Surprisingly, Fe is not correlated to SO_4^{2-}, although jarosite was found in the riverbed. This could indicate that Fe variance is controlled by sequestration in oxy-hydroxides minerals, specifically the observed nanocrystalline goethite, which also could act as a permanent sink for some contaminants like Zn. On the other hand, efflorescent salts represent an important player in the attenuation processes in the dry season, but also a crucial secondary source of pollution in wet seasons, given their high solubility and the high concentrations of metals they can host (Nordstrom, 2011). In this context, seasonal cycles (Nordstrom, 2009) must be taken into account in any future remediation plan.

The approach used in this study could be used in different watersheds worldwide to provide science-based clear information for targeted remediation plans. The study also points out the importance of the comparison of contiguous mining-affected watersheds to highlight the variety of processes influencing the metals cycle and the breadth of contamination sources within the same mining district.

In Rio Montevecchio the contaminant sources were not localised but widespread along the entire study reach, moreover groundwater sources largely contribute to the cumulative loads. Therefore, any remediation action must be taken on a watershed scale rather than localised on the Piccalinna impoundment banks only. In fact, especially the groundwater sources can impede the achievement of positive effects from reclamation (Hancock, 2002; Ward et al., 2001), both in the short and medium time span.

Acknowledgements

The authors acknowledge CESA (grant number: E58C16000080003) from RAS and RAS/FBS (grant number: F72F16003080002) grants, and FP7 ERANETMED2 72094 SUPREME. Additional support was provided by the U.S. Geological Survey's Mineral Resources and Toxic Substances Hydrology Programs. A special thanks goes to Dr. Riccardo Biddau for his precious help with the statistical analysis. Many students from the University of Cagliari provided their help in sampling. Many undergraduate and graduate students from the University of Cagliari provided help in field work. We especially thank Patrizia Onnis for her support in the tracer. The use of brand or trade names in this report is for descriptive purposes only and does not constitute endorsement by the U.S. Geological Survey. We thank AE for handling this manuscript and two referees for their useful comments.

References

Aitchison, J., Greenacre, M., 2002. Biplots of compositional data. Appl. Stat. 51, 375–392. https://doi.org/0035–9254/02/51375

Arslan, C., Arslan, F., 2003. Thermochemical Review of Jarosite and Goethite Stability Regions at 25 and 95 °C. Turkish J. Eng. Environ. Sci. 27, 45–52.

Ashley, R.P., Lloyd, J.W., 1978. An example of the use of factor analysis and cluster analysis in groundwater chemistry interpretation. J. Hydrol. 39, 355–364. https://doi.org/10.1016/0022-1694(78)90011-2

Bacchetta, G., Casti, M., Zavattero, L., 2007. Analisi della vegetazione del distretto minerario di Montevecchio (Sardegna sud-occidentale). Fitosociologia 44, 83–108.

Baron, D., Palmer, C.D., 1996. Solubility of jarosite at 4-35°C, Pergamon Geochimica et Cosmochimica Acta.

Biddau, R., Cidu, R., Da Pelo, S., Carletti, A., Ghiglieri, G., Pittalis, D., 2019. Source and fate of nitrate in contaminated groundwater systems: Assessing spatial and temporal variations by hydrogeochemistry and multiple stable isotope tools. Sci. Total Environ. 647, 1121–1136. https://doi.org/10.1016/j.scitotenv.2018.08.007

Bigham, J.M., Nordstrom, D.K., 2000. Iron and Aluminum Hydroxysulfates from Acid Sulfate Waters. Rev. Mineral. Geochemistry 40, 351–403. https://doi.org/https://doi.org/10.2138/rmg.2000.40.7

Bladh, K.W., 1982. The formation of goethite, jarosite, and alunite during the weathering of sulfide-bearing felsic rocks. Econ. Geol. 77, 176–184. https://doi.org/10.2113/gsecongeo.77.1.176

Buxton, H.T., Nimick, D.A., von Guerard, P., Church, S.E., Frazier, A.., Gray, J.R., Lipin, B.R., Marsh, S.P., Woodward, D.F., Kimball, B.A., Finger, S.E., Ischinger, L.S., Fordham, J.C., Power, M.S., Bunck, C.M., Jones, J.W., 1997. A Science-Based, Watershed Strategy to Support Effective Remediation of Abandoned Mine Lands | USGS Abandoned Mine Land Initiative, in: ICARD Fourth International Conference on Acid Rock Drainage. Vancouver.

Byrne, P., Binley, A., Heathwaite, A.L., Ullah, S., Heppell, C.M., Lansdown, K., Zhang, H., Trimmer, M., Keenan, P., 2014. Control of river stage on the reactive chemistry of the hyporheic zone. Hydrol. Process. 28, 4766–4779. https://doi.org/10.1002/hyp.9981

Byrne, P., Runkel, R.L., Walton-Day, K., 2017. Synoptic sampling and principal components analysis to identify sources of water and metals to an acid mine drainage stream.

Environ. Sci. Pollut. Res. 24, 17220–17240. https://doi.org/10.1007/s11356-017-9038-x

Caboi, R., Cidu, R., Fanfani, L., Lattanzi, P., Zuddas, P., 1999. Environmental mineralogy and geochemistry of the abandoned Pb-Zn Montevecchio-Ingurtosu mining district, Sardinia, Italy. Chron. la rechérche miniére 534, 21–28.

Cao Pinna, C., Silvano, R., Fadda, A., Buffa, F., Orrù, N., 1998. Studio dell'Idrologia Superficiale della Sardegna (SISS). EAF (Ente Autonomo del Flumendosa) - Cagliari.

Cavanagh, P.D., S, B.M., Pratt, L.M., 2017. Efflorescence of Gypsum and Jarosite During Exposure of Sulfidic Lacustrine Sediment, Western Greenland, in: Lunar and Planetary Science Conference XLVIII.

Cidu, R., 2011. Mobility of aqueous contaminants at abandoned mining sites: insights from case studies in Sardinia with implications for remediation. Environ. Earth Sci. 64, 503–512. https://doi.org/10.1007/s12665-010-0874-y

Cidu, R., Dore, E., Biddau, R., Nordstrom, D.K., 2018. Fate of Antimony and Arsenic in Contaminated Waters at the Abandoned Su Suergiu Mine (Sardinia, Italy) . Mine Water Environ. 37, 151–165. https://doi.org/10.1007/s10230-017-0479-8

Cidu, R., Fanfani, L., 2002. Overview of the environmental geochemistry of mining districrs in the southwestern Sardinia, Italy. Geochemistry Explor. Environ. Anal. 2, 243–251.

Cidu, R., Frau, F., da Pelo, S., 2011. Drainage at Abandoned Mine Sites: Natural Attenuation of Contaminants in Different Seasons. Mine Water Environ. 30, 113–126. https://doi.org/10.1007/s10230-011-0146-4

Comas-Cufì, M., Thiò-Henestrosa, S., 2011. CoDaPack 2.0: a stand-alone, multi-platform compositional software., in: Egozcue, J.J., Tolosana-Delgado, R., Ortego, M.I. (Eds.), CoDaWork'11: 4th International Workshop on Compositional Data Analysis. Sant Feliu de Guíxols.

Cuccuru, S., Naitza, S., Secchi, F., Puccini, A., Casini, L., Pavanetto, P., Linnemann, U., Hofmann, M., Oggiano, G., 2016. Structural and metallogenic map of late Variscan Arbus Pluton (SW Sardinia, Italy). J. Maps 12, 860–865. https://doi.org/10.1080/17445647.2015.1091750

De Giudici, G., Medas, D., Cidu, R., Lattanzi, P., Podda, F., Frau, F., Rigonat, N., Pusceddu, C., Da Pelo, S., Onnis, P., Marras, P.A., Wanty, R.B., Kimball, B., 2017a. Application of hydrologic-tracer techniques to the Casargiu adit and Rio Irvi (SW-Sardinia, Italy): Using enhanced natural attenuation to reduce extreme metal loads. Appl. Geochemistry 96, 42–54. https://doi.org/10.1016/j.apgeochem.2018.06.004

De Giudici, G., Medas, D., Meneghini, C., Casu, M.A., Gianoncelli, A., Iadecola, A., Podda,

S., Lattanzi, P., 2015. Microscopic biomineralization processes and Zn bioavailability: a synchrotron-based investigation of *Pistacia lentiscus* L. roots. Environ. Sci. Pollut. Res. 22, 19352–19361. https://doi.org/10.1007/s11356-015-4808-9

De Giudici, G., Pusceddu, C., Medas, D., Meneghini, C., Gianoncelli, A., Rimondi, V., Podda, F., Cidu, R., Lattanzi, P., Wanty, R.B., Kimball, B.A., 2017b. The role of natural biogeochemical barriers in limiting metal loading to a stream affected by mine drainage. Appl. Geochemistry 76, 124–135. https://doi.org/10.1016/j.apgeochem.2016.11.020

De Giudici, G., Wanty, R.B., Podda, F., Kimball, B.A., Verplanck, P.L., Lattanzi, P., Cidu, R., Medas, D., 2014. Quantifying biomineralization of zinc in the Rio Naracauli (Sardinia, Italy), using a tracer injection and synoptic sampling. Chem. Geol. 384, 110–119. https://doi.org/10.1016/j.chemgeo.2014.07.002

Desborough, G.A., Smith, K.S., Lowers, H.A., Swayze, G.A., Hammarstrom, J.M., Diehl, S.F., Leinz, R.W., Driscoll, R.L., 2009. Mineralogical and chemical characteristics of some natural jarosites. Geochim. Cosmochim. Acta 74, 1041–1056. https://doi.org/10.1016/j.gca.2009.11.006

Dold, B., Bernhard, 2014. Evolution of Acid Mine Drainage Formation in Sulphidic Mine Tailings. Minerals 4, 621–641. https://doi.org/10.3390/min4030621

Dunn, J.G., 1997. The oxidation of sulphide minerals. Thermochim. Acta 300, 127–139. https://doi.org/10.1016/S0040-6031(96)03132-2

Elwood Madden, M., Madden, A., Rimstidt, J., Zahrai, S., Kendall, M., Miller, M., 2012. Jarosite dissolution rates and nanoscale mineralogy. Geochim. Cosmochim. Acta 91, 306–321. https://doi.org/10.1016/j.gca.2012.05.001

Figueiredo, M.O., da Silva, T.P., 2011. The positive environmental contribution of jarosite by retaining lead in acid mine drainage areas. Int. J. Environ. Res. Public Health 8, 1575–1582. https://doi.org/10.3390/ijerph8051575

Forray, F.L., Smith, A.M.L., Navrotsky, A., Wright, K., Hudson-Edwards, K.A., Dubbin, W.E., 2014. Synthesis, characterization and thermochemistry of synthetic Pb-As, Pb-Cu and Pb-Zn jarosites. Geochim. Cosmochim. Acta 127, 107–119. https://doi.org/10.1016/j.gca.2013.10.043

Frantisek, M., 2008. Plumbojarosite (Trans)Formation in Lead Contaminated Soil, in: 2008 Joint Meeting of The Geological Society of America, Soil Science Society of America, American Society of Agronomy, Crop Science Society of America, Gulf Coast Association of Geological Societies with the Gulf Coast Section of SEPM.

Frau, F., Medas, D., Da Pelo, S., Wanty, R.B., Cidu, R., 2015. Environmental effects on the

aquatic system and metal discharge to the mediterranean sea from a near-neutral zinc-ferrous sulfate mine drainage. Water. Air. Soil Pollut. 226, 226–255. https://doi.org/10.1007/s11270-015-2339-0

Hancock, P.J., 2002. Human Impacts on the Stream-Groundwater Exchange Zone. Environ. Manage. 29, 763–781. https://doi.org/10.1007/s00267-001-0064-5

Jerz, J.K., Rimstidt, J.D., 2003. Efflorescent iron sulfate minerals: Paragenesis, relative stability, and environmental impact. Am. Mineral. 88, 1919–1932.

Kerolli-Mustafa, M., Ćurković, L., Fajković, H., Rončević, S., 2015. Ecological Risk Assessment of Jarosite Waste Disposal. Croat. Chem. Acta 88, 189–196. https://doi.org/10.5562/cca2554

Kimball, B.A., Runkel, R.L., Walton-Day, K., Bencala, K.E., 2002. Assessment of metal loads in watersheds affected by acid mine drainage by using tracer injection and synoptic sampling: Cement Creek, Colorado, USA. Appl. Geochemistry 17, 1183–1207. https://doi.org/10.1016/S0883-2927(02)00017-3

Kimball, B.A., Walton-Day, K., Runkel, R.L., 2007. Quantification of Metal Loading by Tracer Injection and Synoptic Sampling, 1996–2000 I, in: Church, S.E., von Guerard, P., Finger, S.E. (Eds.), Integrated Investigations of Environmental Effects of Historical Mining in the Animas River Watershed, San Juan County, Colorado. U.S. Geological Survey, pp. 423–488.

Kothe, E., Bergmann, H., Büchel, G., 2005. Molecular mechanisms in bio-geo-interactions: From a case study to general mechanisms. Chemie der Erde - Geochemistry 65, 7–27. https://doi.org/10.1016/j.chemer.2005.06.005

Lambert, P.M., Marston, T., Kimball, B.A., Stolp, B.J., 2011. Assessment of groundwater/surface-water interaction and simulation of potential streamflow depletion induced by groundwater withdrawal, Uinta River near Roosevelt, Utah, Scientific Investigations Report 2011-5044.

Larocque, A.C.L., Rasmussen, P.E., 1998. An overview of trace metals in the environment, from mobilization to remediation. Environ. Geol. 33, 85–91. https://doi.org/10.1007/s002540050227

Lottermoser, B.G., 2010. Tailings, in: Mine Wastes. pp. 205–241. https://doi.org/https://doi.org/10.1007/978-3-642-12419-8_4

Ma, Y., Oliveira, R.S., Freitas, H., Zhang, C., 2016. Biochemical and Molecular Mechanisms of Plant-Microbe-Metal Interactions: Relevance for Phytoremediation. Front. Plant Sci. 7, 1–19. https://doi.org/10.3389/fpls.2016.00918

Majzlan, J., Navrotsky, A., Schwertmann, U., 2004. Thermodynamics of iron oxides: Part III. Enthalpies of formation and stability of ferrihydrite (~$Fe(OH)_3$), schwertmannite (~$FeO(OH)_{3/4}(SO_4)_{1/8}$), and ε-$Fe_2O_3$. Geochim. Cosmochim. Acta 68, 1049–1059. https://doi.org/10.1016/S0016-7037(03)00371-5

Medas, D., De Giudici, G., Casu, M.A., Musu, E., Gianoncelli, A., Iadecola, A., Meneghini, C., Tamburini, E., Sprocati, A.R., Turnau, K., Lattanzi, P., 2015. Microscopic processes ruling the bioavailability of Zn to roots of *Euphorbia Pithyusa* L. Pioneer plant. Environ. Sci. Technol. 49, 1400–1408. https://doi.org/10.1021/es503842w

Medas, D., De Giudici, G., Podda, F., Meneghini, C., Lattanzi, P., 2014. Apparent energy of hydrated biomineral surface and apparent solubility constant: An investigation of hydrozincite. Geochim. Cosmochim. Acta 140, 349–364. https://doi.org/10.1016/j.gca.2014.05.019

Medas, D., De Giudici, G., Pusceddu, C., Casu, M.A., Birarda, G., Vaccari, L., Gianoncelli, A., Meneghini, C., 2019. Impact of Zn excess on biomineralization processes in *Juncus acutus* grown in mine polluted sites. J. Hazard. Mater. 370, 98–107. https://doi.org/10.1016/j.jhazmat.2017.08.031

Merroun, M.L., 2007. Interactions between Metals and Bacteria: Fundamental and Applied Research. Commun. Curr. Res. Educ. Top. Trends Appl. Microbiol. 4, 108–119.

Nordstrom, D.K., 2011. Hydrogeochemical processes governing the origin, transport and fate of major and trace elements from mine wastes and mineralized rock to surface waters. Appl. Geochemistry 26, 1777–1791. https://doi.org/10.1016/j.apgeochem.2011.06.002

Nordstrom, D.K., 2009. Acid rock drainage and climate change. J. Geochemical Explor. 100, 97–104. https://doi.org/10.1016/j.gexplo.2008.08.002

Nordstrom, D.K., 1977. Thermochemical redox equilibria of ZoBell's solution. Geochim. Cosmochim. Acta 41, 1835–1841. https://doi.org/https://doi.org/10.1016/0016-7037(77)90215-0

Orange, H., 2008. Industrial Archaeology: Its Place Within the Academic Discipline, the Public Realm and the Heritage Industry. Ind. Archaeol. Rev. 30, 83–95. https://doi.org/10.1179/174581908X347292

Parkhurst, B.D.L., Appelo, C. a J., 1999. User's Guide To PHREEQC (version 2) — a Computer Program for Speciation, and Inverse Geochemical Calculations. Exch. Organ. Behav. Teach. J. D, 326. https://doi.org/Rep. 99-4259

Pawlowsky-Glahn, V., Buccianti, A., 2011. Compositional data analysis : theory and applications. Wiley.

Pisu, R., Serra, S., Demuru, S., Demuru, L., Bertocchi, A.F.F., Persod, P., Dessì, R., Pilurzu, S., Zillo, E., Demuru, S., Bertocchi, A.F.F., Persod, P., Dessì, R., Pilurzu, S., Zillo, E., 2008. Piano Di Bonifica Delle Aree Minerarie Dismesse Del Sulcis-Iglesiente-Guspinese.

PROGEMISA, 1998. Progetto Montevecchio Ingurtosu, Piano di recupero dell'area mineraria dismessa, Indagine sulle componenti ambientali, acqua e suoli e analisi dei fattori di rischio- Relazione, Allegato n. 5.

Pusceddu, C., 2013. Studio dei materiali del bacino fanghi della miniera di Montevecchio Levante: processi mineralogici e dispersione dei metalli pesanti. Università degli Studi di Cagliari.

Rimondi, V., Costagliola, P., Gray, J.E., Lattanzi, P., Nannucci, M., Paolieri, M., Salvadori, A., 2014. Mass loads of dissolved and particulate mercury and other trace elements in the Mt. Amiata mining district, Southern Tuscany (Italy). Environ. Sci. Pollut. Res. 21, 5575–5585. https://doi.org/10.1007/s11356-013-2476-1

Romano, E., De Giudici, G., Bergamin, L., Andreucci, S., Maggi, C., Pierfranceschi, G., Celia Magno, M., Ausili, A., 2017. The marine sedimentary record of natural and anthropogenic contribution from the Sulcis-Iglesiente mining district (Sardinia, Italy). Mar. Pollut. Bull. 122, 331–343. https://doi.org/10.1016/j.marpolbul.2017.06.070

Runkel, R.L., Walton-Day, K., Kimball, B.A., Verplanck, P.L., Nimick, D.A., 2013. Estimating instream constituent loads using replicate synoptic sampling, Peru Creek, Colorado. J. Hydrol. 489, 26–41. https://doi.org/10.1016/j.jhydrol.2013.02.031

Schwertmann, U., Taylor, R.M., 1972. The Transformation of Lepidocrocite to Goethite. Clays Clay Miner. 20, 151–158.

Taggart, J.E., 2002. Analytical methods for chemical analysis of geologic and other materials, U.S. Geol. Survey Open-File Report 02-0223.

Templ, M., Filzmoser, P., Reimann, C., 2008. Cluster analysis applied to regional geochemical data: Problems and possibilities. Appl. Geochemistry 23, 2198–2213. https://doi.org/10.1016/J.APGEOCHEM.2008.03.004

Ward, J.V., Tockner, K., Uehlinger, U., Malard, F., 2001. Understanding natural patterns and processes in river corridors as the basis for effective river restoration. Regul. Rivers Res. Manag. 17, 311–323. https://doi.org/10.1002/rrr.646.abs

Table

Figure 1. Map of the Montevecchio area with the location of the sampling points, boreholes, adit and mining areas. The instream samples are divided in the four sub-reaches identified by the statistical analysis.

Figure 2: Rio Montevecchio along the banks of Piccalinna impoundment. In the streambed ochreous Fe precipitates are visible, whereas on the embankment white-grey efflorescent minerals are present.

Table 1. Calculated discharge, pH and major components of synoptic samples (filtered) of Rio Montevecchio stream waters. D.L. for HCO_3^- set to 5 mg/l. * Italian law decree D.lgs 152/06

Table 2: Trace chemical components of synoptic samples of Rio Montevecchio stream waters. * Italian law decree D.lgs 152/06

Figure 3: (a) instream pH spatial profile and pH values of inflow waters. The four sub-reaches and the injection point represent the five clusters of instream synoptic samples identified by the cluster analysis (b) Piper diagram of stream waters of Rio Montevecchio and its inflows. Zn was included among the main cations because of its high concentrations. Grouping of Instream samples is based on the results of cluster analysis, with the Injection point corresponding to cluster 1; RBIs refer to the right bank inflows, whereas LBIs to the left bank inflows.

Figure 4: Spatial profiles of contaminant concentration in non-filtered (blue lines) and filtered (black lines) instream and inflow (red circles) water samples. The vertical dashed blue represents the main inflow (Rio Struvoniga – L2)

Figure 5: Compositional clr-biplot showing the relationship between mean values of Rio Montevecchio stream waters (a) and inflows (b). Both diagrams show variables (rays) and observations (circles).

Table

Table 1.

	Discharge	**SO_4**	**SO_4 load**	**Zn**	**Zn load**	**Fe(F)**	**Fe(F) load**	**Mn**	**Mn load**
	l/s	mg/l	kg/day	mg/l	kg/day	mg/l	kg/day	mg/l	kg/day
03/06/13	11.19	1640	1547	300	271	30	29	48	46
25/05/15	6.06	1600	859	280	157	26	14	52	27

Table

Figure 1. Map of the Montevecchio area with the location of the sampling points, boreholes, adit and mining areas. The instream samples are divided in the four sub-reaches identified by the statistical analysis.

Figure 2: Rio Montevecchio along the banks of Piccalinna impoundment. In the streambed ochreous Fe precipitates are visible, whereas on the embankment white-grey efflorescent minerals are present.

Figure 3: (a) instream pH spatial profile and pH values of inflow waters. The four sub-reaches and the injection point represent the five clusters of instream synoptic samples identified by the cluster analysis (b) Piper diagram of stream waters of Rio Montevecchio and its inflows. Zn was included among the main cations because of its high concentrations. Grouping of Instream samples is based on the results of cluster analysis, with the Injection point corresponding to cluster 1; RBIs refer to the right bank inflows, whereas LBIs to the left bank inflows.

Figure 4: Spatial profiles of contaminant concentration in non-filtered (blue lines) and filtered (black lines) instream and inflow (red circles) water samples. The vertical dashed blue represents the main inflow (Rio Struvoniga – L2)

Figure 5: Compositional clr-biplot showing the relationship between mean values of Rio Montevecchio stream waters (a) and inflows (b). Both diagrams show variables (rays) and observations (circles).

Figure 6: Br concentration and calculated discharge vs. distance in the synoptic samples. Blue dashed lines show the position of the inflows.

Figure 7: Difference between cumulative and instream loads. All loads are calculated from filtered samples, with the exception of Fe (TOT) and Al, calculated from the unfiltered sample. The coloured boxes represent four Sub-reaches identified by the CA analysis.

Table 1: Comparison of discharge, contaminants concentration and calculated loads between the synoptic point MV-1133 (3rd of June 2013) and slug at MV-1182 (25th of May 2015).

Figure

Click here to download high resolution image

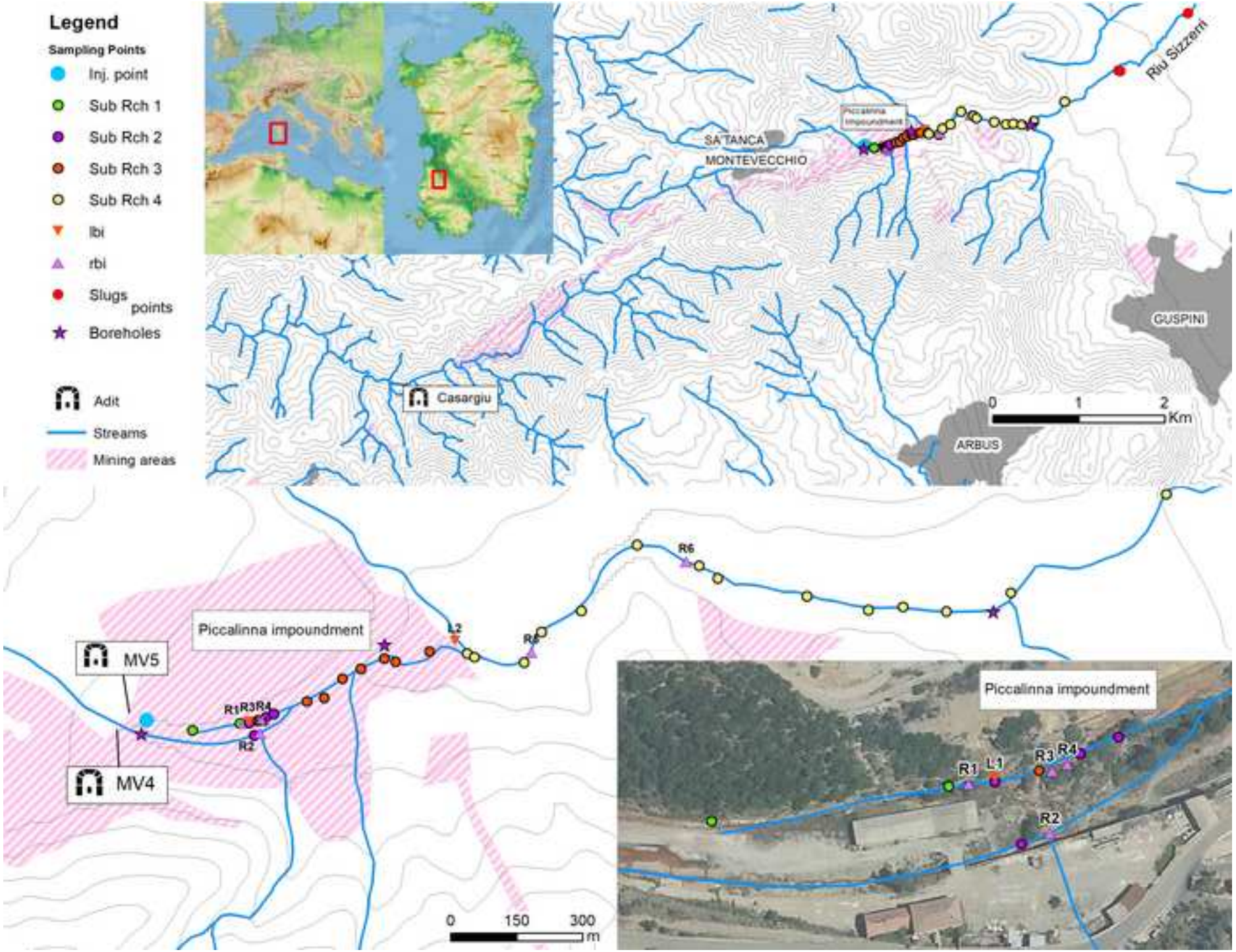

Figure

Click here to download high resolution image

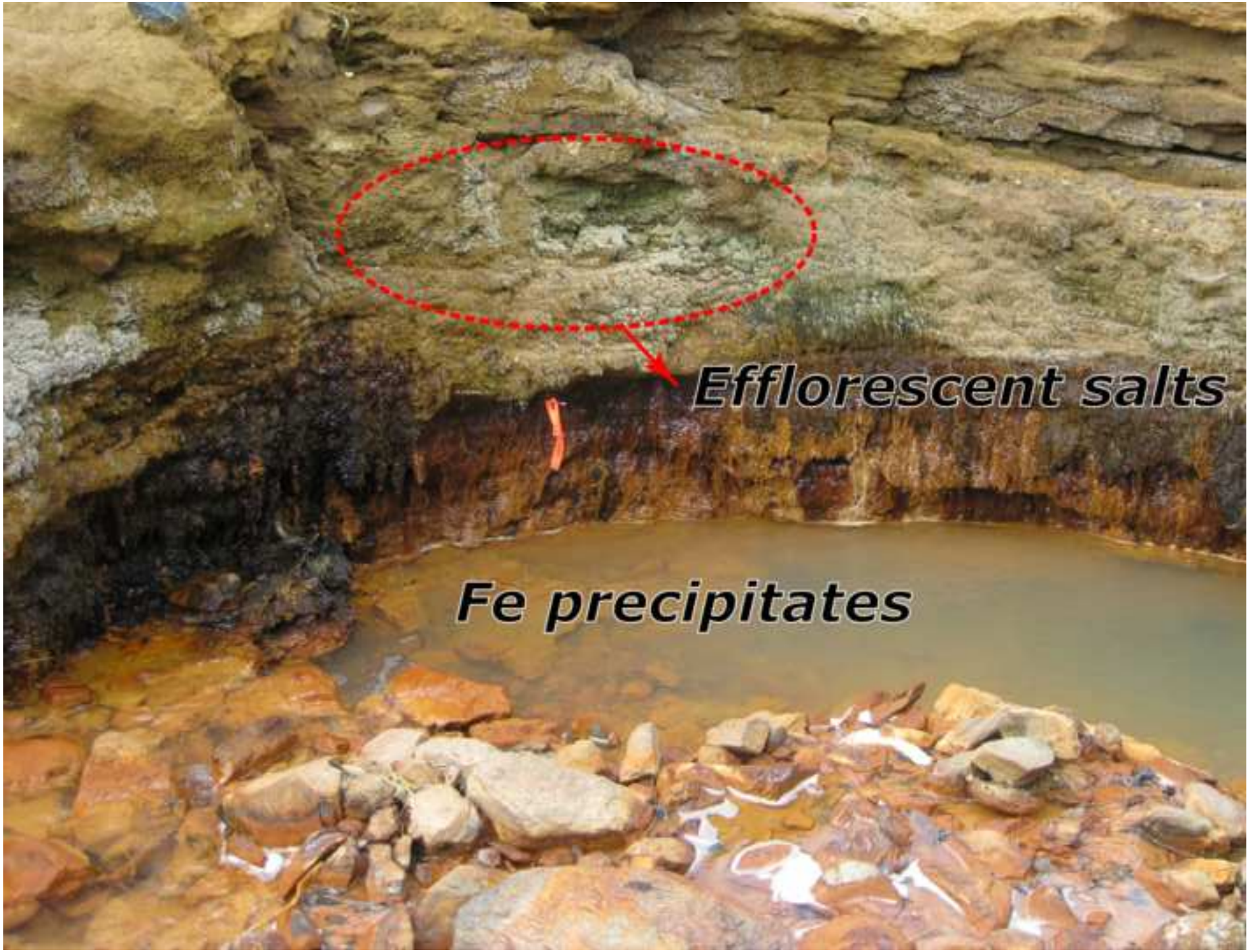

Figure

Click here to download high resolution image

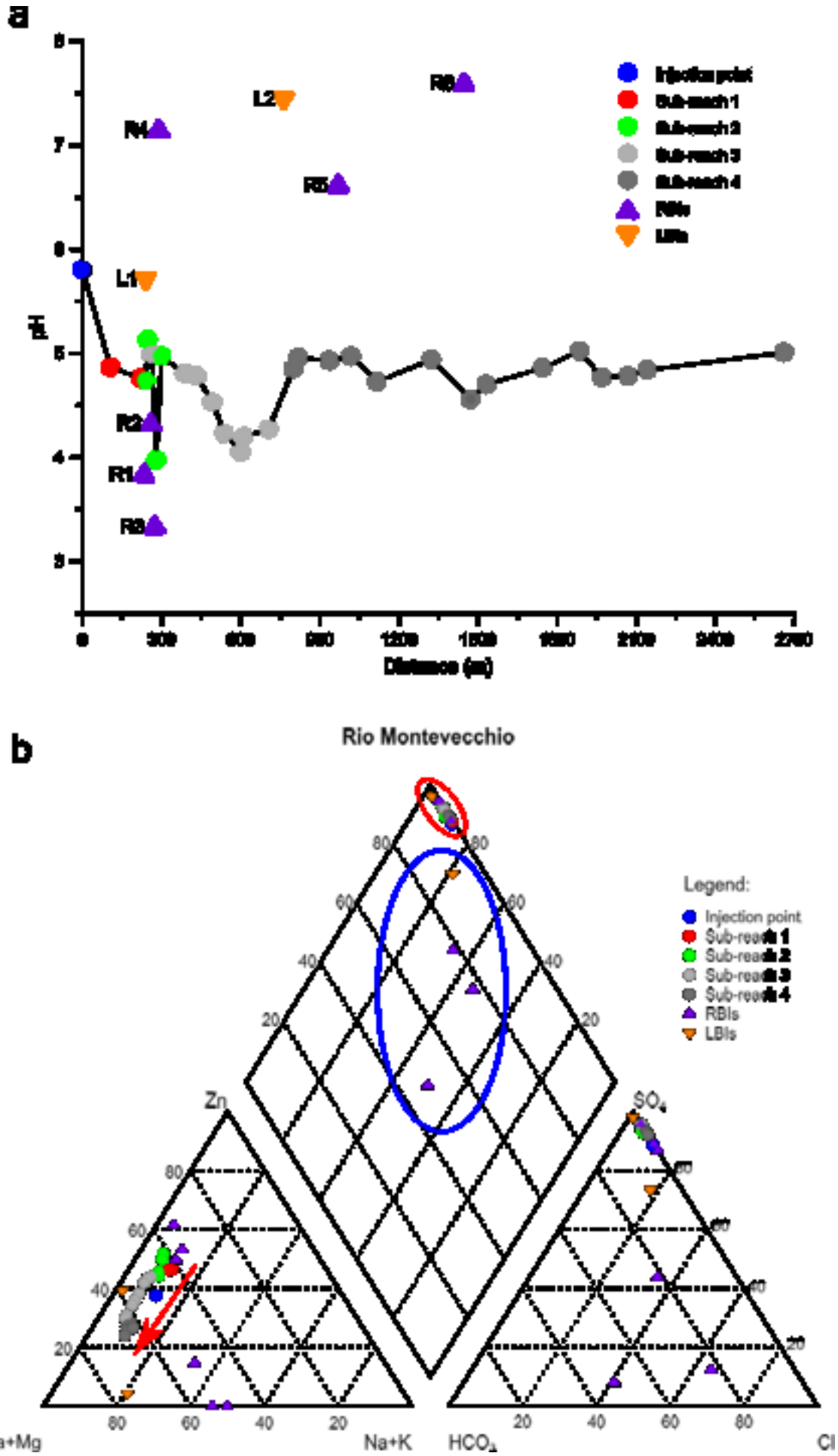

Figure

Click here to download high resolution image

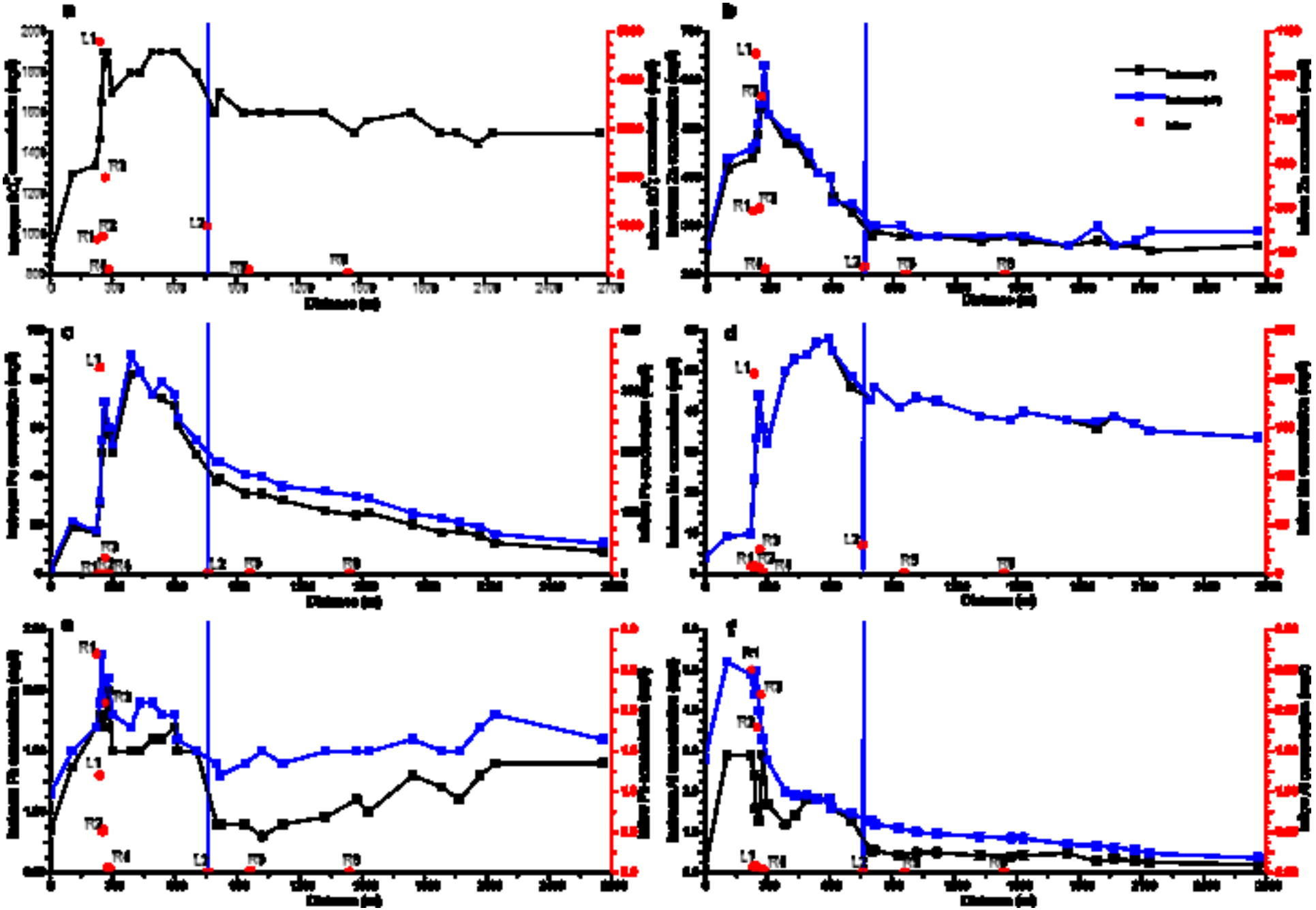

Figure

Click here to download high resolution image

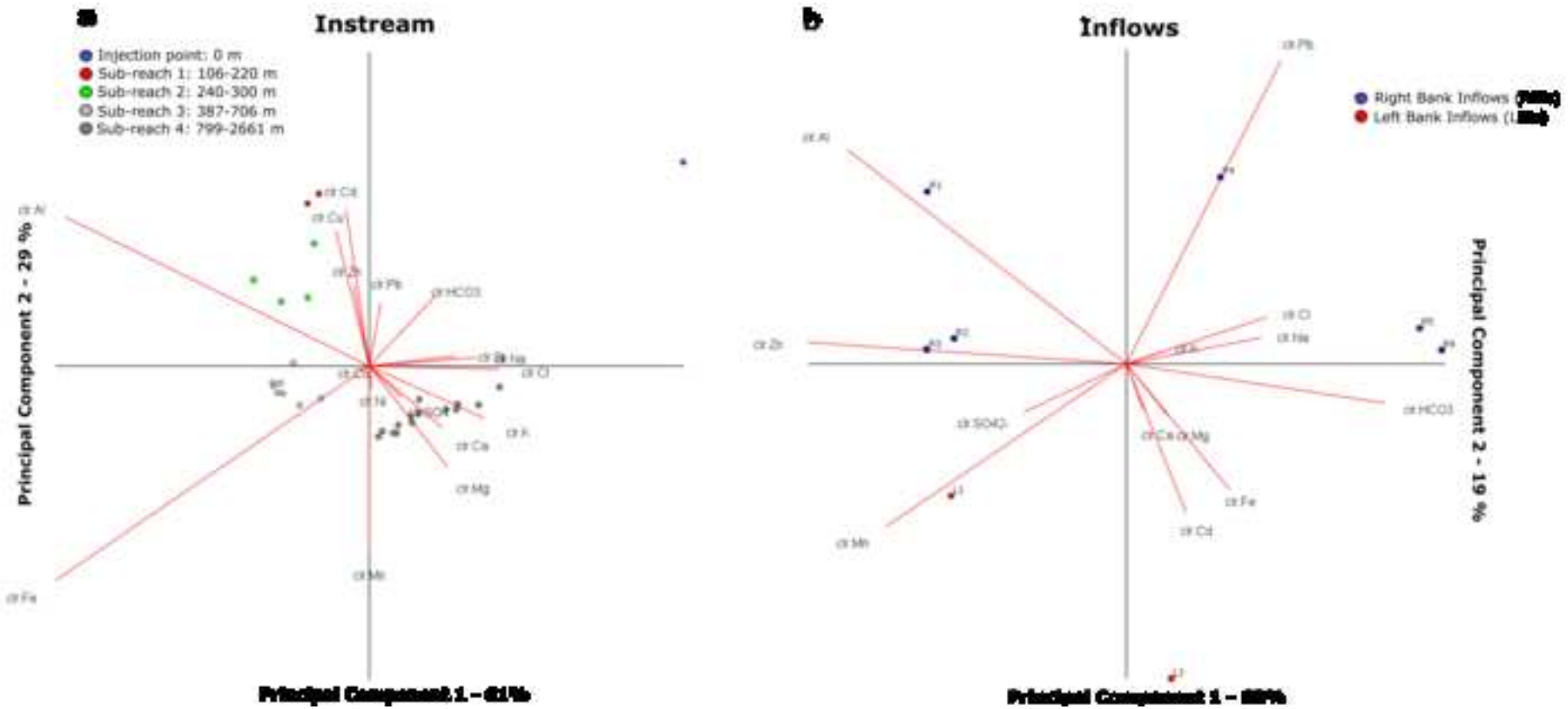

Figure

Click here to download high resolution image

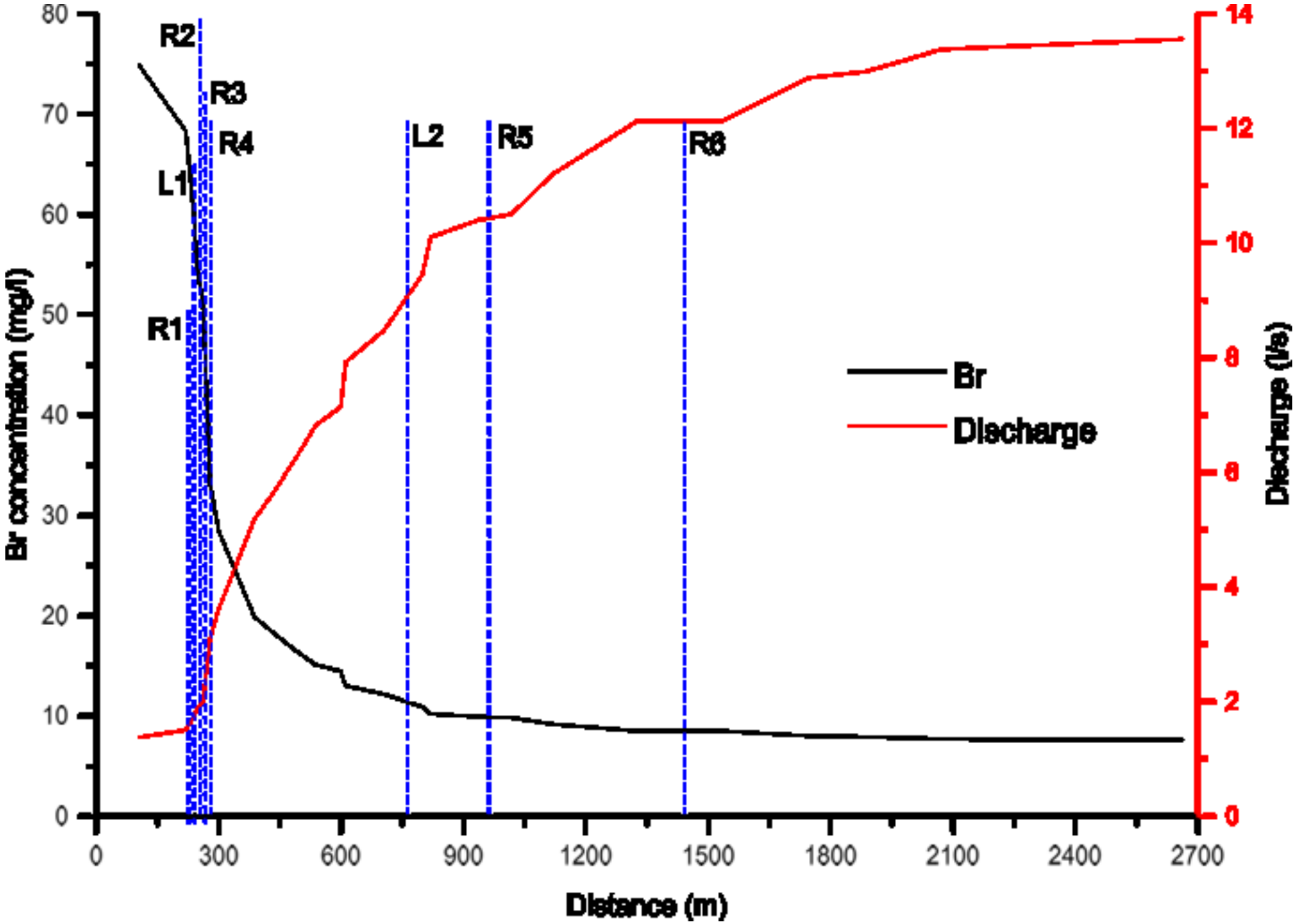

Figure

Click here to download high resolution image

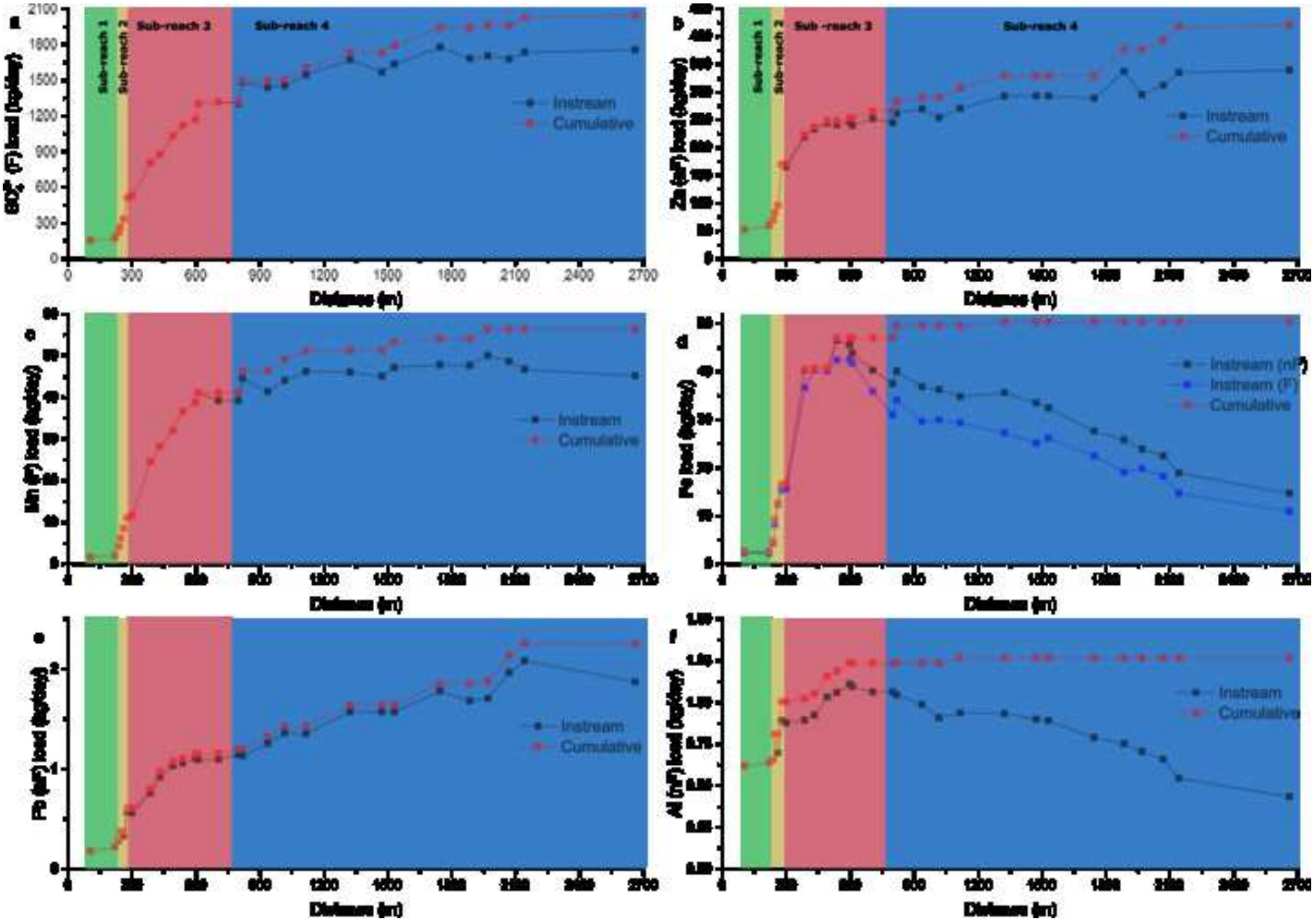

Supplementary material

Assessment of origin and fate of contaminants along mining-affected Rio Montevecchio (SW Sardinia, Italy): a hydrologic-tracer and environmental mineralogy study.

Giovanni De Giudici[a,*], Daniela Medas[a], Rosa Cidu[a], Pierfranco Lattanzi[b], Nicola Rigonat[a], Ilaria Frau[c], Francesca Podda[a], Pier Andrea Marras[a], Elisabetta Dore[a], Franco Frau[a], Valentina Rimondi[d] Robert L. Runkel[e], Richard B. Wanty[f], Briant Kimball[g]

[a]Department of Chemical and Geological Sciences, University of Cagliari, Cittadella Universitaria, Monserrato, 09042 (CA - Italy)

[b]CNR-IGG, UOS Firenze, via La Pira 4, Firenze, I-50121, Italy

[c]Built Environment and Sustainable Technologies (BEST) Research Institute, Liverpool John Moores University, Liverpool L3 3AF, UK

[d]Dipartimento di Scienze della Terra, Università di Firenze, via La Pira 4, Firenze, I-50121, Italy

[e]U.S. Geological Survey, Colorado Water Science Center, 3215 Marine St, Bldg 6 Boulder, CO, 80303

[f]U.S. Geological Survey, MS 964d Denver Federal Center, Denver, CO 80225

[g]U.S. Geological Survey, 2329 W Orton Circle, Salt Lake City, Utah, 84117

*corresponding author: gbgiudic@unica.it

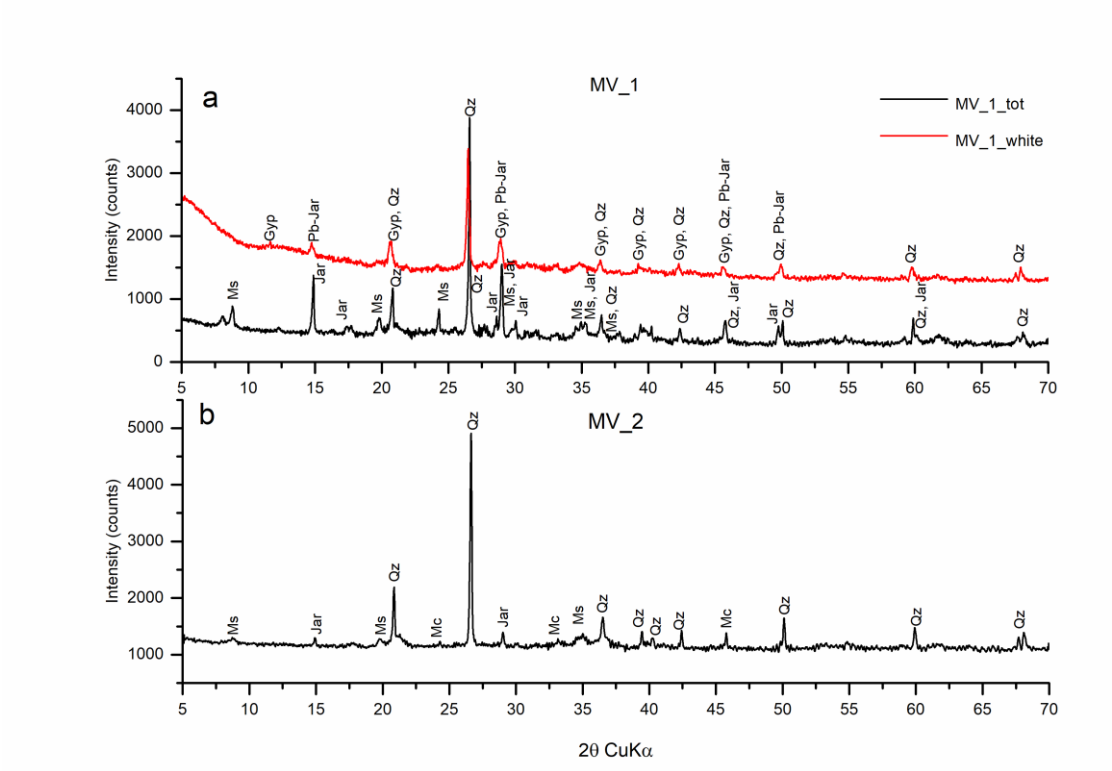

Figure S1. XRPD traces of wet precipitates sampled in Rio Montevecchio streambed (MV_1_white was a white crust appeared after drying) and in R3 streambed (MV_2). Ms: muscovite, Jar: jarosite, Qz: quartz, Gyp: gypsum, Pb-jar: plumbojarosite, Mc: microcline.

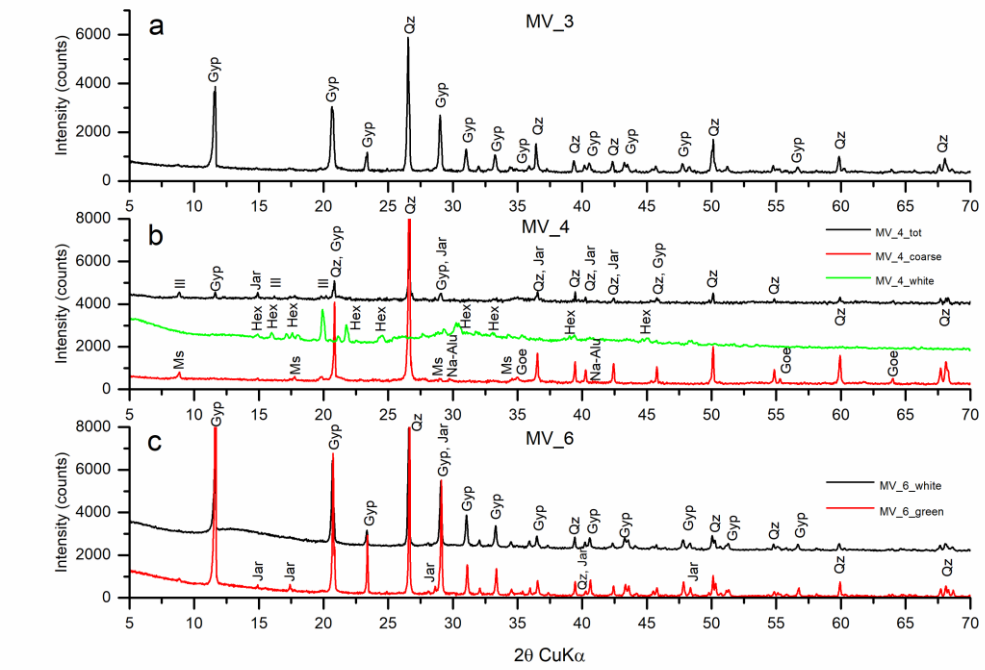

Figure S2. XRPD traces of precipitates sampled in Rio Montevecchio dry streambed (MV_4 and MV_6) 50 meters downstream from the point shown in Figure 2. MV_3 is the white efflorescence visible in Figure 2. MV_4_white and MV_6_white are a white crust formed upon complete drying of the humid sediment. Ms: muscovite, Jar: jarosite, Qz: quartz, Gyp: gypsum, Ill: Illite, Hex: hexahydrite, Goe: goethite.

Table S1. Calculated Inflow load (ΔM_i) for the Rio Montevecchio Inflows.

ID	Code	Distance	SO_4^{2-}	Zn	Fe	Mn	Al	Pb
		(m)	kg/day	kg/day	kg/day	kg/day	kg/day	kg/day
MV-230 RBI F	R1	227	13.5	5.4	0.001	0.16	0.05	0.05
MV-242 LBI F	L1	240	65	13.6	4.6	2.8	0.001	0.016
MV-260 RBI F	R2	255	9.7	3.6	0	0.09	0.021	0.006
MV-283 RBI F	R3	266	190	77	2.4	2.37	0.21	0.2
MV-303 RBI F	R4	282	5.6	1.2	0	0.02	0.001	0.003
MV-793 LBI F	L2	762	84	3.2	0	2.5	0	0
MV-979 RBI F	R5	963	0.8	0.007	0.0001	0.001	0	0.0001
MV-1437 RBI F	R6	1441	0	0	0	0	0	0

Table S2. Calculated discharge, pH and major components of synoptic samples (filtered) of Rio Montevecchio stream waters. D.L. for HCO3- set to 5 mg/l. * Italian law decree D.lgs 152/06.

Site ID	Distance	Cluster	Q	pH	Eh	Ca	Mg	Na	K	HCO_3	Cl	SO_4^{2-}	Zn
	m		l/s		mV	mg/l	mg/l	mg/l	mg/l	mg/l	mg/l	mg/l	mg/l
MV-0000	0	1	1.37	5.85	473	118	54	53	5.1	5,6	82	890	250
MV-0110	106	2	1.37	4.87	468.9	133	60	73	4.2	<D.L.	79	1,300	420
MV-0220	220	2	1.5	4.76	472.6	149	61	70	5.0	<D.L.	78	1,340	440
MV-0240	240	3	1.7	4.74	456.6	174	74	65	4.9	15	76	1,470	460
MV-0255	247	3	1.87	5.13	470.7	160	86	63	4.5	19	71	1,650	490
MV-0280	262	4	2.01	4.99	490.9	216	91	61	5.2	<D.L.	71	1,900	540
MV-0300	279	3	3.12	3.98	600.9	168	86	55	4.7	nd	68	1,900	630
MV-0323	300	3	3.62	4.97	502.4	150	78	53	4.3	<D.L.	68	1,700	530
MV-0413	387	4	5.17	4.81	494.8	176	95	49	4.8	<D.L.	65	1,800	470
MV-0456	433	4	5.62	4.78	499.5	191	101	49	4.9	<D.L.	63	1,800	470
MV-0516	492	4	6.28	4.53	517.4	203	106	51	5.3	<D.L.	65	1,900	430
MV-0564	538	4	6.82	4.23	535	212	114	52	5.7	<D.L.	64	1,900	410
MV-0621	599	4	7.13	4.05	569.3	221	120	53	6.1	<D.L.	66	1,900	400
MV-0650	612	4	7.92	4.2	589.9	231	128	55	7.1	<D.L.	65	1,900	360
MV-0731	706	4	8.47	4.27	587	229	119	54	6.5	<D.L.	68	1,800	330
MV-0818	799	5	9.45	4.85	461.8	209	120	64	6.7	<D.L.	83	1,600	280
MV-0837	819	5	10.1	4.96	476.8	210	119	64	6.5	<D.L.	80	1,700	290
MV-0951	937	5	10.4	4.93	478.7	200	116	61	6.4	<D.L.	84	1,600	280
MV-1031	1018	5	10.5	4.97	469.7	223	116	66	6.8	<D.L.	86	1,600	280
MV-1133	1117	5	11.19	4.73	488	200	115	66	6.7	<D.L.	88	1,600	280
MV-1329	1324	5	12.12	4.94	503.7	199	114	67	6.8	<D.L.	86	1,600	270
MV-1469	1473	5	12.12	4.56	469.3	195	113	67	6.7	<D.L.	87	1,500	280
MV-1520	1532	5	12.12	4.7	498.6	195	109	64	6.2	<D.L.	86	1,560	270
MV-1726	1745	5	12.87	4.86	504.8	205	112	68	6.2	<D.L.	92	1,600	260
MV-1869	1886	5	12.98	5.02	488.9	199	113	71	6.7	<D.L.	93	1,500	270
MV-1948	1970	5	13.16	4.77	498.6	193	110	69	6.7	<D.L.	94	1,500	260
MV-2048	2070	5	13.38	4.78	505.2	194	112	71	6.7	<D.L.	94	1,450	260
MV-2200	2142	5	13.39	4.84	502.6	241	110	71	6.7	<D.L.	92	1,500	250
MV-2800	2661	5	13.55	5.01	510.9	191	110	72	6.7	<D.L.	96	1,500	260
	Surface water discharge limits*			5.5-9.5			-	-	-	-	1,200	1,000	0.5

Table S3. Trace chemical components of synoptic samples of Rio Montevecchio stream waters. * Italian law decree D.lgs 152/06

Site ID	Mn	Fe (F)	Fe(nF)	Cd	Pb	Al	Co	Ni	Cu
	mg/l	mg/l	mg/l	µg/l	µg/l	µg/l	µg/l	µg/l	µg/l
MV-0000	9	0.4	1.9	2,000	850	58	180	340	340
MV-0110	14	19	22	3,500	1,370	2,900	290	510	470
MV-0220	15	17	18	3,700	1,700	2,900	310	540	530
MV-0240	28	29	30	3,600	1,800	2,400	360	630	530
MV-0255	38	50	55	3,600	1,800	1,600	420	750	470
MV-0280	49	71	71	3,400	1,700	1,300	490	870	470
MV-0300	41	57	60	4,600	2,000	2,900	460	850	810
MV-0323	37	50	53	3,600	1,500	1,700	410	740	690
MV-0413	55	82	90	2,900	1,500	1,200	440	840	490
MV-0456	58	83	83	2,700	1,500	1,400	470	860	500
MV-0516	59	74	74	2,400	1,600	1,800	460	850	460
MV-0564	62	72	79	2,200	1,600	1,800	460	880	430
MV-0621	63	69	74	2,200	1,700	1,800	470	890	430
MV-0650	60	61	64	1,900	1,500	1,600	420	810	380
MV-0731	51	49	55	1,800	1,500	1,300	360	700	330
MV-0818	48	38	46	1,600	900	540	340	670	270
MV-0837	51	39	46	1,500	900	540	330	630	270
MV-0951	46	33	41	1,500	900	430	320	620	250
MV-1031	49	33	40	1,500	800	500	310	630	260
MV-1133	48	30	36	1,500	900	500	300	610	250
MV-1329	44	26	34	1,400	960	430	290	590	240
MV-1469	43	24	32	1,500	1,100	410	300	590	240
MV-1520	45	25	31	1,500	1,000	430	290	590	240
MV-1726	43	20	25	1,400	1,300	490	280	590	250
MV-1869	41	17	23	1,400	1,200	279	280	550	220
MV-1948	44	17	21	1,400	1,100	330	290	580	240
MV-2048	42	16	19	1,460	1,300	300	280	570	220
MV-2200	40	13	16	1,400	1,400	250	260	520	200
MV-2800	39	9.3	12	1,400	1,400	210	270	540	220
Surface water discharge limits*	2	2	-	20	200	1000	-	2000	100

Table S4. Discharge, pH and major components of synoptic samples (filtered) of waters of the inflows of Rio Montevecchio. D.L. for HCO_3^- set to 5 mg/l.

ID	Code	Distance	pH	Ca	Mg	Na	K	HCO_3	Cl	SO_4^{2-}
		(m)		mg/l	mg/l	mg/l	mg/l	mg/l	mg/l	mg/l
MV-230 RBI F	R1	227	3.84	67	32	41	3.5	nd	82	730
MV-242 LBI F	L1	240	5.72	508	250	28	7.6	65.48	33	4,800
MV-260 RBI F	R2	255	4.33	83	38	45	4.7	<D.L.	73	800
MV-283 RBI F	R3	266	3.34	178	58	41	4.9	nd	64	2,000
MV-303 RBI F	R4	282	7.15	30	17	42	2.7	79.83	75	128
MV-793 LBI F	L2	762	7.45	204	125	126	6.5	150.15	180	1,000
MV-979 RBI F	R5	963	6.62	80	56	164	5.6	235	390	100
MV-1437 RBI F	R6	1441	7.60	38	24	88	1	259.91	120	32

Table S5. Trace chemical components of synoptic samples (filtered) of waters of the inflows of Rio Montevecchio. D.L. for Al is set at 3 µg/l and for Fe at 20 µg/l.

ID	Code	Distance	Zn	Mn	Fe	Cd	Pb	Al	Co	Ni	Cu
		(m)	mg/l	mg/l	mg/l	µg/l	µg/l	µg/l	µg/l	µg/l	µg/l
MV-230 RBI F	R1	227	290	8	0.060	2,380	2,700	2,500	170	290	940
MV-242 LBI F	L1	240	1,000	206	340	2,700	1,200	80	1,400	2,600	22
MV-260 RBI F	R2	255	300	7	<D.L.	2,600	520	1,800	120	300	700
MV-283 RBI F	R3	266	810	25	25	7,000	2,100	2,200	470	810	1,700
MV-303 RBI F	R4	282	27	0.5	<D.L.	260	60	30	8.8	30	54
MV-793 LBI F	L2	762	38	30	<D.L.	77	<D.L.	<D.L.	120	260	2.4
MV-979 RBI F	R5	963	0.8	0.1	16	5.6	15	<D.L.	1	2	8
MV-1437 RBI F	R6	1441	0.09	0.03	<D.L.	1.5	1.9	<D.L.	0.21	0.79	2.1

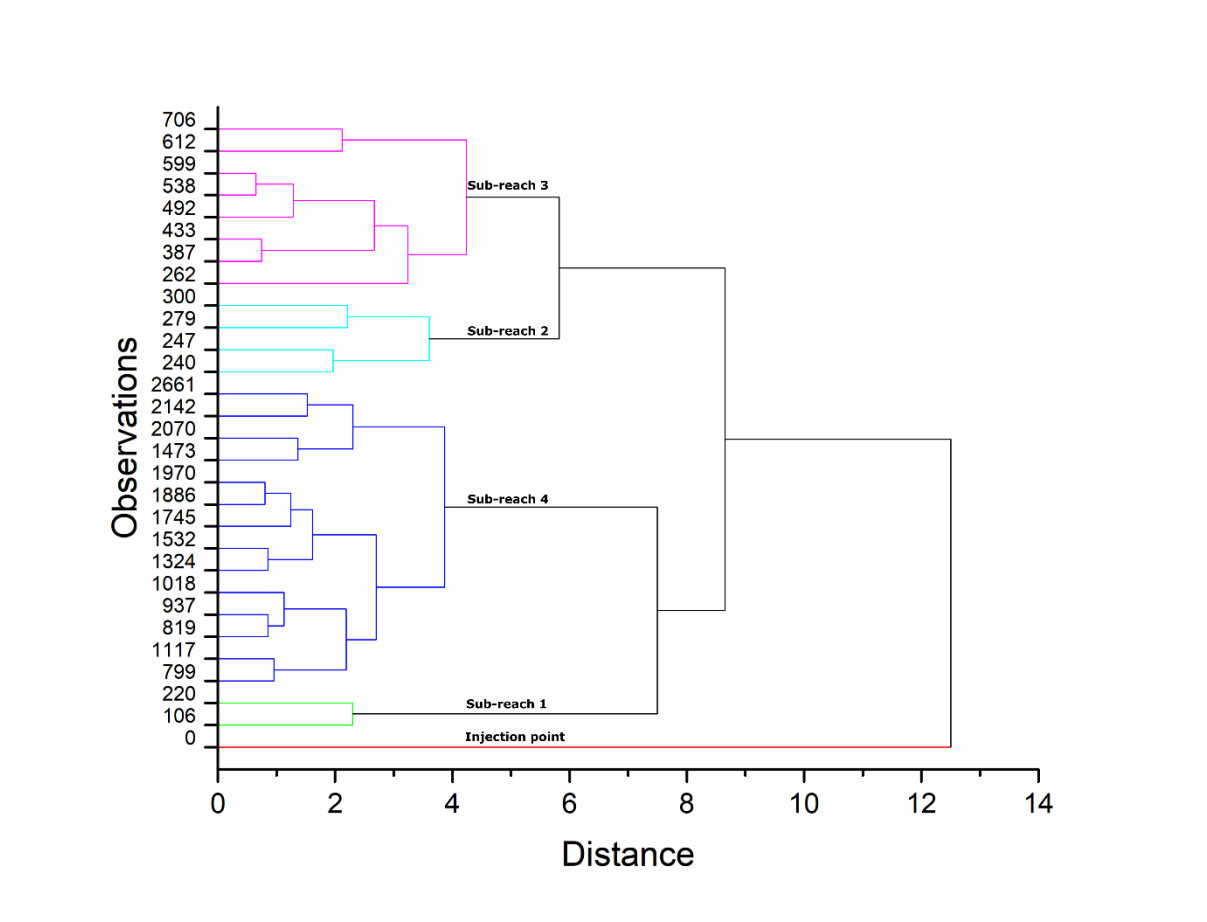

Figure S3. Dendrogram representing the results of the hierarchical cluster analysis (CA) performed on compositional data of Rio Montevecchio instream waters. The four sub-reaches and the Injection point represent the five clusters identified by the analysis.

Table S6. Calculated ΔM_S values and results of calculation of Cumulative Load, Instream Load and Net Attenuation. The grey-shaded boxes indicate the segments that are the most important source areas for the given contaminant.

ID	Distance	Reach	$\Delta M_S\ SO_4^{2-}$	ΔM_S Zn	ΔM_S Mn	ΔM_S Fe (TOT)	ΔM_S Fe (F)	ΔM_S Al	ΔM_S Pb
MV-0110	106	1	48.8	22.6	0.6	2.3	2.2	0.612	0.08
MV-0220	220	1	19.9	7.6	0.3	-0.3	-0.1	0.020	0.04
MV-0240	240	2	44.2	10.0	2.3	2.1	2.1	0.016	0.06
MV-0255	247	2	49.2	12.9	2.0	4.5	3.8	0.157	0.09
MV-0280	262	3	63.6	13.2	2.3	3.5	4.3	-0.114	-0.04
MV-0300	279	2	180.9	73.9	2.5	3.8	3.0	0.192	0.23
MV-0323	300	2	20.3	-3.8	0.5	0.4	0.3	-0.013	0.00
MV-0413	387	3	272.3	53.1	13.0	23.6	21.0	0.017	0.20
MV-0456	433	3	70.4	14.3	3.6	0.1	3.7	0.030	0.16
MV-0516	492	3	155.7	10.8	3.8	-0.2	-0.2	0.107	0.11
MV-0564	538	3	88.8	-2.6	4.5	6.4	2.3	0.030	0.03
MV-0621	599	3	51.2	4.9	2.3	-1.0	0.1	0.048	0.05
MV-0650	612	3	129.7	-6.9	2.2	-1.8	-0.8	-0.014	-0.01
MV-0731	706	3	17.7	13.1	-1.9	-3.5	-5.9	-0.033	0.00
MV-0818	799	4	-12.1	-7.8	0.0	-2.7	-4.9	-0.001	0.04
MV-0837	819	4	176.9	16.8	5.3	2.6	3.0	-0.014	-0.01
MV-0951	937	4	-44.9	7.9	-3.1	-3.3	-4.4	-0.058	0.12
MV-1031	1018	4	13.2	-15.7	2.7	-0.6	0.3	-0.082	0.10
MV-1133	1117	4	96.2	16.8	2.1	-1.5	-0.6	0.031	-0.01
MV-1329	1324	4	127.5	22.3	-0.1	0.8	-2.1	-0.006	0.22
MV-1469	1473	4	-104.7	0.0	-1.0	-2.1	-2.1	-0.031	0.00
MV-1520	1532	4	62.8	0.0	2.1	-1.0	1.0	-0.010	0.00
MV-1726	1745	4	146.6	-3.9	0.7	-4.9	-3.7	-0.100	0.21
MV-1869	1886	4	-130.2	47.4	-0.1	-1.8	-3.4	-0.038	-0.10
MV-1948	1970	4	56.3	-41.0	2.3	-1.9	0.8	-0.047	0.02
MV-2048	2070	4	-30.1	16.4	-1.5	-1.5	-1.6	-0.046	0.26
MV-2200	2142	4	60.5	23.6	-1.8	-3.6	-3.6	-0.115	0.12
MV-2800	2661	4	20.1	3.9	-1.6	-4.2	-3.8	-0.111	-0.21
Cumulative Load			2,078	421	56.33	50.4	48	1.27	2.25
Instream Load			1,756	340	45.2	14.6	10.9	0.43	1.87
Net Attenuation			288 (14%)	81 (19%)	11.3 (20%)	35.4 (70%)	37 (77%)	0.84 (66%)	0.38 (17%)

Table S7. Values for the saturation indices (S.I.) for green rust II ($Fe_6(OH)_{12}(SO_4)$:$8H_2O$), schwertmannite ($FeO(OH)_{0.75}(SO_4)_{0.125}$), ferrihydrite ($Fe(OH)_3$), Jarosite ($KFe_3(SO_4)_2(OH)_6$), anglesite ($PbSO_4$), hemimorphite ($Zn_4Si_2O_7(OH)_2$:$H_2O$, amorphous $Al(OH)_3$ and gibbsite ($Al(OH)_3$). Grey boxes indicate the samples belonging to sub-reach 4, where most of Fe and Al attenuation occurs.

Site ID	Distance	GR(II)	Schwertmannite	Ferrihydrite	Jarosite	Anglesite	Hemimorphite	$Al(OH)_3$	Gibbsite
	m	S.I	S.I	S.I.	S.I	S.I	S.I	S.I	S.I.
MV-0000	0	-15.71	3.46	2.72	1.47	-0.62	6.78	-1.02	1.74
MV-0110	106	-13.09	2.92	1.93	2.34	-0.39	-0.27	-1.85	0.89
MV-0220	220	-14.72	2.62	1.6	1.76	-0.29	-0.99	-2.19	0.55
MV-0240	240	-14.47	2.53	1.5	1.47	-0.27	-1.17	-2.41	0.33
MV-0255	247	-8.03	4.03	3.1	5.16	-0.26	1.97	-1.47	1.27
MV-0280	262	-8.19	4.13	3.16	5.89	-0.26	0.95	-2	0.74
MV-0300	279	-17.22	3.13	1.91	5.12	-0.19	-6.83	-4.66	-1.91
MV-0323	300	-8.09	4.09	3.11	5.84	-0.33	0.77	-1.77	0.95
MV-0413	387	-8.52	3.76	2.75	5.4	-0.33	-0.83	-2.37	0.35
MV-0456	433	-9.26	3.78	2.76	5.38	-0.33	-1.07	-2.48	0.25
MV-0516	492	-11.81	3.35	2.26	4.75	-0.29	-3.27	-3.12	-0.39
MV-0564	538	-14.58	2.81	1.65	3.9	-0.3	-5.75	-3.97	-1.25
MV-0621	599	-15.69	2.87	1.66	4.51	-0.28	-7.23	-4.49	-1.77
MV-0650	612	-14.25	3.53	2.36	6.15	-0.32	-6.24	-4.16	-1.43
MV-0731	706	-14.12	3.57	2.42	6.07	-0.32	-5.7	-4.03	-1.3
MV-0818	799	-11.5	3.01	2.01	3.05	-0.56	-1.2	-2.65	0.08
MV-0837	819	-9.28	3.67	2.7	4.7	-0.55	-0.11	-2.23	0.49
MV-0951	937	-10.76	3.37	2.38	3.99	-0.55	-0.92	-2.6	0.12
MV-1031	1018	-9.89	3.49	2.52	4.13	-0.61	-0.13	-2.24	0.49
MV-1133	1117	-13.02	2.95	1.91	3.2	-0.55	-2.42	-3.13	-0.4
MV-1329	1324	-10.73	3.66	2.67	4.89	-0.52	-0.98	-2.61	0.12
MV-1469	1473	-15.38	2.27	1.2	1.34	-0.48	-3.15	-3.48	-0.76
MV-1520	1532	-13.18	3.04	2	3.44	-0.51	-2.54	-3.19	-0.46
MV-1726	1745	-11.79	3.46	2.46	4.36	-0.39	-1.33	-2.67	0.06
MV-1869	1886	-10.86	3.56	2.6	4.27	-0.44	0.08	-2.42	0.31
MV-1948	1970	-13.29	3.08	2.06	3.4	-0.47	-1.96	-3.08	-0.36
MV-2048	2070	-13.25	3.17	2.15	3.62	-0.41	-1.78	-3.08	-0.35
MV-2200	2142	-13.24	3.18	2.18	3.54	-0.37	-1.48	-2.99	-0.26
MV-2800	2661	-12.15	3.59	2.62	4.39	-0.37	-0.07	-2.58	0.15